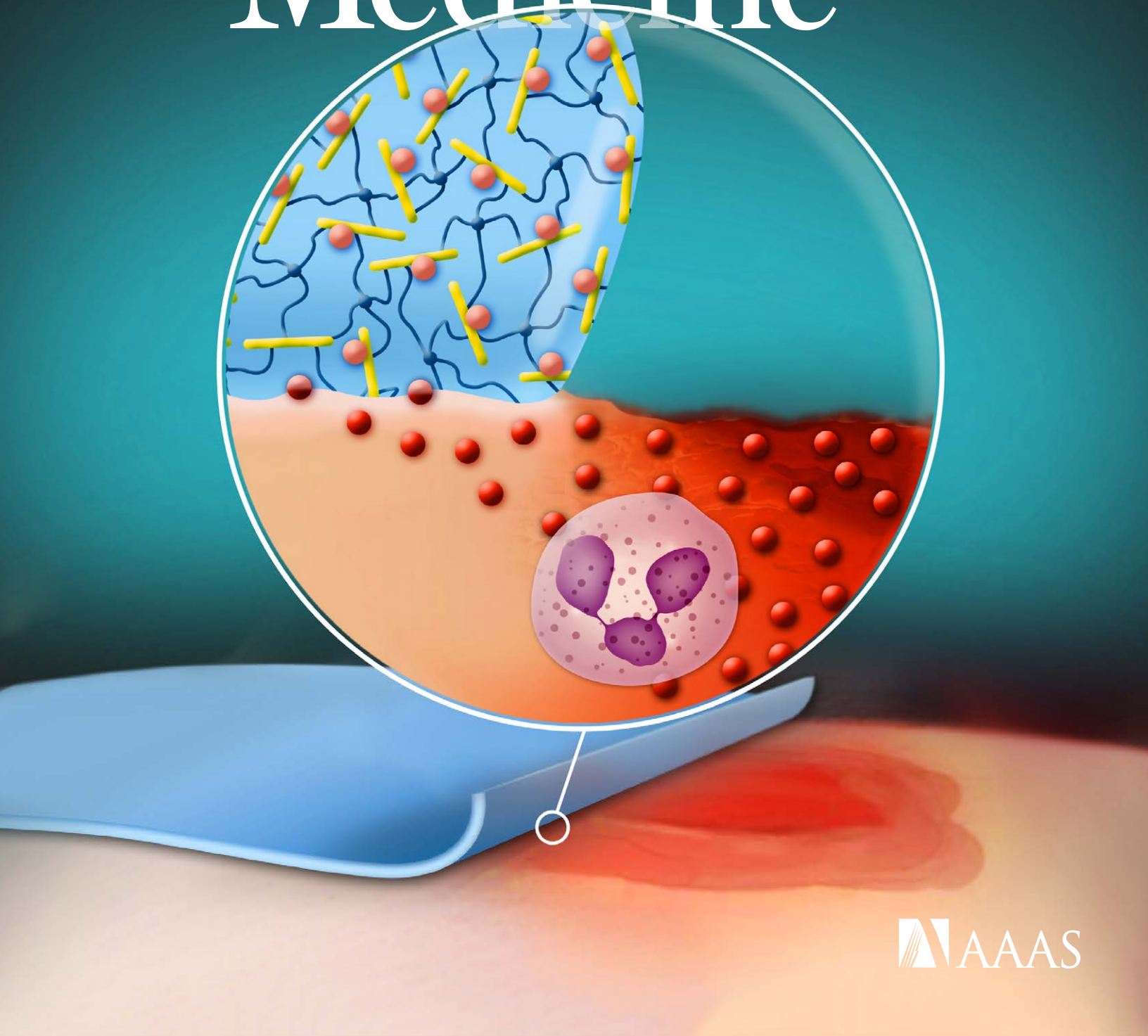


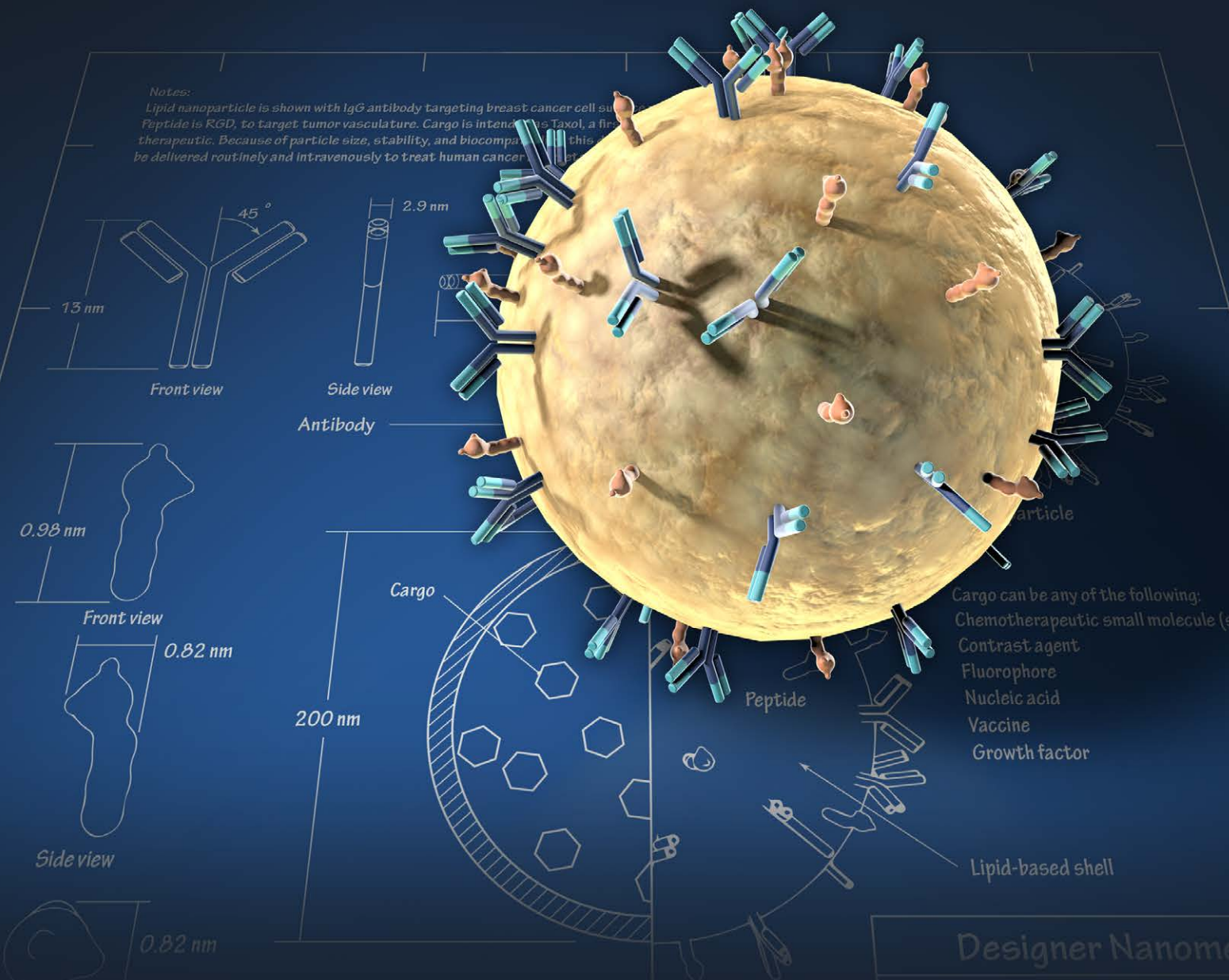
Science Translational Medicine



Make Your Research Hit the Target

Notes:

Lipid nanoparticle is shown with IgG antibody targeting breast cancer cell surface. Peptide is RGD, to target tumor vasculature. Cargo is intended as Taxol, a first-line anticancer drug. Because of particle size, stability, and biocompatibility, this nanoparticle can be delivered routinely and intravenously to treat human cancer.



Science Translational Medicine publishes peer-reviewed, cutting-edge biomedical research in the fields of cardiology, cancer, immunotherapy, infectious diseases and vaccines, bioengineering and devices, neurology and neurodegenerative diseases, obesity, diabetes and metabolic disorders, drug discovery, genomic medicine, imaging, stem cell therapy and regenerative medicine.

Submit your research today

Learn more at: ScienceTranslationalMedicine.org

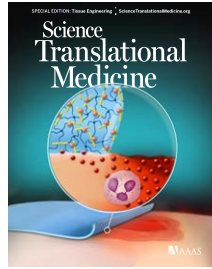
Designer Nanome

2013
**Science
 Translational
 Medicine**



SPECIAL EDITION: Tissue Engineering

Select research published in *Science Translational Medicine*



This image shows a heparin glycosaminoglycan-modified hydrogel applied to a skin wound, where it sequesters chemokines secreted by immune cells. The hydrogel captured inflammatory chemokines from human venous leg ulcer wound fluid and hastened tissue formation and wound closure in a mouse model of delayed skin healing.

Credit: Zoltán Tanczik/Vtur GmbH and Lucas Schirmer, Uwe Freudenberg, Carsten Werner/Leibniz Institute of Polymer Research Dresden

Citation: *Sci Transl. Med.* 10.1126/scitranslmed.aai9044 (2017).

Science Translational Medicine | AAAS

Science Translational Medicine is an interdisciplinary journal that publishes translational research with impact for human health that fills the knowledge gaps between preclinical studies and clinical applications.

Chief Scientific Advisors

Elazer R. Edelman, M.D., Ph.D.

Massachusetts Institute of Technology

Garret A. FitzGerald, M.D.

University of Pennsylvania

Editor

Orla M. Smith, Ph.D.

Editorial Team

Catherine A. Charneski, Ph.D.

Caitlin A. Czajka, Ph.D.

Mattia Maroso, Ph.D.

Yevgeniya Nusinovich, M.D., Ph.D.

Lindsey Pujanandez, Ph.D.

Scientific Advisory Board

James Beeson, MB BS, Ph.D.

Burnet Institute

Sonja M. Best, Ph.D.

National Institute of Allergy and Infectious Diseases
National Institutes of Health

Bruce Blazar, M.D.

University of Minnesota

Jeff Bluestone, Ph.D.

UCSF Diabetes Center

Tania Bubela, J.D., Ph.D.

Simon Fraser University

Martine D. Clozel, M.D.

Actelion Pharmaceuticals Ltd.

Jacob Corn, Ph.D.

University of California at Berkeley

Grégoire Courtine, Ph.D.

Center for Neuroprosthetics and Brain Mind
Institute, Swiss Federal Institute of Technology
(EPFL)

Michele De Palma, Ph.D.

Ecole Polytechnique Fédérale de Lausanne (EPFL)
Swiss Federal Institute of Technology, Lausanne

Steven Deeks, M.D.

University of California, San Francisco

Sudhansu K. Dey, Ph.D.

Cincinnati Children's Hospital Medical Center

Luis Diaz Jr., M.D.

Memorial Sloan Kettering Cancer Center

Harry C. Dietz, M.D.

Johns Hopkins University School of Medicine

Georg N. Duda, Ph.D.

Charité Universitätsmedizin, Berlin

Sabine A. Eming, M.D.

University of Cologne

Padraic Fallon, Ph.D, D.Sc.

Trinity Biomedical Sciences Institute
Trinity College Dublin

Thomas Fehr, M.D.

University of Zurich

Mark C. Fishman, M.D.

Novartis Institutes for Biomedical Research

Scott L. Friedman, M.D.

Mount Sinai School of Medicine

Sanjiv Sam Gambhir, M.D., Ph.D.

Stanford University School of Medicine

Geoffrey S. Ginsburg, M.D., Ph.D.

Duke Institute for Genome Sciences & Policy

Jeffrey I. Gordon, M.D.

Washington University in St. Louis,
School of Medicine

Frank Harrell Jr., Ph.D.

Vanderbilt University School of Medicine

Marc Hellerstein, M.D., Ph.D.

University of California at Berkeley

Eric Hoffman, Ph.D.

Revergen BioPharma
Binghamton University – SUNY

Elaine Holmes, Ph.D.

Imperial College London

David Holtzman, M.D.

Washington University School of Medicine

Kenya Honda, M.D. Ph.D.

Keio University School of Medicine

Gökhan S. Hotamisligil, M.D., Ph.D.

Harvard University, School of Public Health

Steven E. Hyman, M.D.

Harvard Medical School

Carl H. June, M.D.

University of Pennsylvania

Stephen F. Kingsmore, MB, ChB, BAO,

DSc, FRCPath

Rady Pediatric Genomic and
Systems Medicine Institute

Marina Konopleva, M.D., Ph.D.

The University of Texas MD Anderson Cancer Center

Robert Langer, Ph.D.

Massachusetts Institute of Technology

Elizabeth M. McNally, M.D., Ph.D.

Northwestern University

Lisa M. McShane, Ph.D.

National Cancer Institute and National Institutes
of Health

Bernard Munos, MBA, M.S.

InnoThink Center for Research in Biomedical
Innovation

Gary Nabel, M.D., Ph.D.

Sanofi-Aventis

Carl Nathan, M.D.

Weill Cornell Medicine

Alan Packer, Ph.D.

Simons Foundation

Leonard Petrucelli, Ph.D.

Mayo Clinic College of Medicine

Kornelia Polyak, M.D., Ph.D.

Harvard Medical School

Glenn Prestwich, Ph.D.

The University of Utah

Rino Rappuoli, Ph.D.

Novartis Vaccines and Diagnostics

Jeremy N. Rich, M.D., MHS, MBA

University of California, San Diego

José-Alain Sahel, M.D.

Pierre and Marie Curie University
National Eye Hospital
INSERM-UPMC
University of Pittsburgh Medical Center (USA)

Padmanee Sharma, M.D., Ph.D.

The University of Texas MD Anderson Cancer Center

Gerald I. Shulman, M.D., Ph.D.

Howard Hughes Medical Institute
Yale University

G. Sitta Sittampalam, Ph.D.

NCATS, NIH

Jean Paul Thiery, Ph.D.

National University of Singapore

Eric J. Topol, M.D.

Scripps Translational Science Institute

Gordana Vunjak-Novakovic, Ph.D.

Columbia University

Ralph Weissleder, M.D., Ph.D.

Massachusetts General Hospital
Harvard Medical School

David S. Wilkes, M.D.

University of Virginia School of Medicine

Tadataka (Tachi) Yamada, M.D.

Frazier Healthcare

Keith R. Yamamoto, Ph.D.

University of California, San Francisco

Peter Zandstra, Ph.D.

University of Toronto

Elias Zerhouni, M.D.

Sanofi-Aventis

IN THIS BOOKLET

RESEARCH ARTICLE

4 SPINAL CORD INJURY

Survival of syngeneic and allogeneic iPSC-derived neural precursors after spinal grafting in minipigs

Jan Strnad et al. (Martin Marsala)

RESEARCH ARTICLE ABSTRACTS

19 Mechanobiologically optimized 3D titanium-mesh scaffolds enhance bone regeneration in critical segmental defects in sheep

Anne-Marie Pobloth et al. (Philipp Schwabe)

Synthetic biology-based cellular biomedical tattoo for detection of hypercalcemia associated with cancer

Aizhan Tastanova et al. (Martin Fussenegger)

20 Computational modeling guides tissue-engineered heart valve design for long-term in vivo performance in a translational sheep model

Maximilian Y. Emmert et al. (Simon P. Hoerstrup)

Production and transplantation of bioengineered lung into a large animal model

Joan E. Nichols et al. (Joaquin Cortiella)

Publisher / Science family of journals: **Bill Moran**
AD/Business Development: **Justin Sawyers**
Marketing Manager: **Shawana Arnold**
Layout/Design: **Kim Huynh**

SPINAL CORD INJURY

Survival of syngeneic and allogeneic iPSC-derived neural precursors after spinal grafting in minipigs

Jan Strnad^{1,2}, Cassiano Carromeu³, Cedric Bardy^{4,5}, Michael Navarro¹, Oleksandr Platoshyn¹, Andreas N. Glud¹, Silvia Marsala¹, Jozef Kafka¹, Atsushi Miyanohara^{1,6}, Tomohisa Kato Jr.⁷, Takahiro Tadokoro¹, Michael P. Hefferan¹, Kota Kamizato¹, Tetsuya Yoshizumi¹, Stefan Juhas⁸, Jana Juhasova⁸, Chak-Sum Ho⁹, Taba Kheradmand⁹, PeiXi Chen¹, Dasa Bohaciakova^{1,10}, Marian Hruska-Plochan^{1,11}, Andrew J. Todd¹², Shawn P. Driscoll¹³, Thomas D. Glenn¹³, Samuel L. Pfaff¹³, Jiri Klima⁸, Joseph Ciacci¹⁴, Eric Curtis¹⁴, Fred H. Gage⁴, Jack Bui¹⁵, Kazuhiko Yamada¹⁶, Alysson R. Muotri³, Martin Marsala^{1,17*}

Copyright © 2018
The Authors, some
rights reserved;
exclusive licensee
American Association
for the Advancement
of Science. No claim
to original U.S.
Government Works

The use of autologous (or syngeneic) cells derived from induced pluripotent stem cells (iPSCs) holds great promise for future clinical use in a wide range of diseases and injuries. It is expected that cell replacement therapies using autologous cells would forego the need for immunosuppression, otherwise required in allogeneic transplantations. However, recent studies have shown the unexpected immune rejection of undifferentiated autologous mouse iPSCs after transplantation. Whether similar immunogenic properties are maintained in iPSC-derived lineage-committed cells (such as neural precursors) is relatively unknown. We demonstrate that syngeneic porcine iPSC-derived neural precursor cell (NPC) transplantation to the spinal cord in the absence of immunosuppression is associated with long-term survival and neuronal and glial differentiation. No tumor formation was noted. Similar cell engraftment and differentiation were shown in spinally injured transiently immunosuppressed swine leukocyte antigen (SLA)-mismatched allogeneic pigs. These data demonstrate that iPSC-NPCs can be grafted into syngeneic recipients in the absence of immunosuppression and that temporary immunosuppression is sufficient to induce long-term immune tolerance after NPC engraftment into spinally injured allogeneic recipients. Collectively, our results show that iPSC-NPCs represent an alternative source of transplantable NPCs for the treatment of a variety of disorders affecting the spinal cord, including trauma, ischemia, or amyotrophic lateral sclerosis.

INTRODUCTION

The technology for generating induced pluripotent stem cells (iPSCs) (1, 2) has opened new possibilities for patient-specific cell therapy, in vitro disease modeling, and drug discovery. Although disease-specific iPSCs provide an excellent tool for studying the developmental pathology of human diseases in vitro (3, 4), the use of iPSCs for spinal cord autologous, syngeneic, or allogeneic transplantation has rarely been tested in large-animal models. The use of large-animal models that show similarities in spinal cord and central nervous system (CNS) anatomy and function with humans is necessary for advancing cell transplantation therapies using iPSC technology to a clinical setting.

Given the ethical issues related to the use of primates, pigs serve as an alternative model for preclinical experiments in regenerative medicine (5, 6). However, isolation of embryonic stem cells (ESCs) from pigs is difficult and not effective (7). Several groups reported successful generation of pig iPSCs, but the engraftment properties of autologous or syngeneic iPSC-derived neural precursors once grafted back into CNS were rarely explored (8–11). Therefore, we sought to test the immunogenicity and engraftment properties of iPSC-derived lineage-committed NPCs, which are expected to be free of pluripotent cell contaminants and, therefore, not form teratoma-like tumor masses.

Here, we analyze syngeneic transplantations of pig NPCs derived from swine leukocyte antigen (SLA)-inbred pig iPSCs. NPCs were isolated by manual clone selection, expanded, and characterized before transplantation. Three months after transplantation into the spinal cord of syngeneic recipients in the absence of immunosuppression, NPCs showed robust engraftment and neuronal/glial differentiation without detectable rejection or tumor formation. In addition, a comparable degree of cell engraftment and differentiation was observed after allogeneic transplantation in transiently immunosuppressed pigs with previous chronic spinal traumatic injury. No detectable presence of circulating anti-iPSC-NPC antibodies was seen in iPSC-NPC-grafted nonimmunosuppressed syngeneic or transiently immunosuppressed allogeneic pigs.

These data demonstrate the lack of immunogenicity of iPSC-NPCs engrafted into naïve noninjured or spinal trauma-injured spinal cord. In addition, the successful engraftment observed in allogeneic animals receiving only time-limited immunosuppression indicates a potential for clinical utilization of human iPSC-NPCs in patients with a different human leukocyte antigen signature.

¹Neuroregeneration Laboratory, Department of Anesthesiology, University of California, San Diego (UCSD), La Jolla, CA 92037, USA. ²Biomedical Center Martin, Department of Molecular Medicine, Jessenius Faculty of Medicine in Martin, Comenius University in Bratislava, 03601 Martin, Slovakia. ³Department of Pediatrics, UCSD, La Jolla, CA 92037, USA. ⁴Laboratory of Genetics, The Salk Institute for Biological Studies, La Jolla, CA 92037, USA. ⁵Laboratory for Human Neurophysiology and Genetics, South Australian Health & Medical Research Institute (SAHMRI) Mind and Brain, Adelaide, South Australia, Australia. ⁶Vector Development Core Laboratory, UCSD, La Jolla, CA 92093, USA. ⁷Center for iPSC Cell Research and Application (CIRA), Kyoto University, Kyoto, Japan. ⁸Institute of Animal Physiology and Genetics, v.v.i., The Czech Academy of Sciences, Liběchov, Czech Republic. ⁹Histocompatibility Laboratory, Gift of Life Michigan, Ann Arbor, MI 48108, USA. ¹⁰Department of Histology and Embryology, Masaryk University, Brno, Czech Republic. ¹¹Institute of Molecular Life Sciences, University of Zurich, Winterthurerstrasse 190, 8057 Zurich, Switzerland. ¹²Institute of Neuroscience and Psychology, College of Medical, Veterinary and Life Sciences, University of Glasgow, Glasgow G12 8QQ, UK. ¹³Gene Expression Laboratory and the Howard Hughes Medical Institute, Salk Institute for Biological Studies, La Jolla, CA 92037, USA. ¹⁴Department of Neurosurgery, UCSD, La Jolla, CA 92103, USA. ¹⁵Department of Pathology, UCSD, La Jolla, CA 92093, USA. ¹⁶Columbia University Medical Center Campus, New York, NY 10032, USA. ¹⁷Institute of Neurobiology, Slovak Academy of Sciences, Kosice, Slovakia.

*Corresponding author. Email: mmarsala@ucsd.edu

RESULTS**NPCs derived from reprogrammed adult porcine skin fibroblasts generate functional neurons in vitro**

We first generated the porcine iPSC-NPCs. Four fully SLA-matched adult pigs were used to obtain skin biopsies (Fig. 1A). All tissue explants successfully produced fibroblasts (Fig. 1B) and pluripotent colonies (Fig. 1, C and D) after reprogramming using Sendai vectors (*12*) encoding octamer-binding transcription factor 4 (*OCT4*), (sex-determining region Y)-box 2 (*SOX2*), Kruppel-like factor 4 (*KLF4*), and myelocytomatosis viral oncogene (*c-MYC*). Expression of the pluripotent markers such as *KLF4*, *SOX2*, *OCT4*, and *Nanog* homeobox (*NANOG*) was seen in proliferating iPSC colonies (Fig. 1, E to H). Previously frozen iPSCs (passages 12 to 18) showed a comparable formation of pluripotent colonies and expression of pluripotent markers (fig. S1, A to F).

To test the differentiation potential of established iPSCs, three different in vitro or in vivo assays were used. First, proliferating colonies were induced to form embryoid bodies (EBs) (Fig. 1I) and continuously cultured in the presence of pig serum (0.1 to 1%) for 3 to 4 weeks. Second, a single monolayer of iPSCs was induced using established germ layer-specific (ectoderm, endoderm, or mesoderm) induction protocols for 10 to 14 days. After induction, EBs and induced iPSCs were stained with markers of mesoderm (smooth muscle actin and brachyury), endoderm [α -fetoprotein (AFP) and sex-determining region Y (*SOX17*)], and ectoderm [orthodenticle homeobox 2 (*OTX2*) and neuron-specific class III β -tubulin (*TUJ1*)]. Third, a single cell suspension of iPSCs was injected into the testes of immunodeficient mice, and the presence of teratomas was analyzed at 4 to 8 weeks after injection. Staining of in vitro-induced EBs (fig. S1, G to J) or induced single cell-seeded iPSCs (fig. S1, K to M) shows the expression of definitive ectoderm, endoderm, and mesoderm markers. Macroscopic inspection of iPSC-injected testes showed extensive bilateral tumor formation at intervals longer than 5 weeks after cell injection (fig. S1N, left bottom, black-background inset). Hematoxylin and eosin (H&E) staining of histological sections taken from injected testes showed developed teratomas with all three germ layer derivatives (Fig. 1J and fig. S1N).

To generate NPCs, we cultured EBs in the presence of basic fibroblast growth factor (bFGF) to potentiate the formation of neural rosettes (Fig. 1K). NPCs were then manually harvested from the periphery of neural rosettes. NPCs were further expanded with bFGF as a sole mitogen (10 ng/mg) for up to 35 passages (Fig. 1L) with expression of neural precursor markers including *SOX2*, type VI intermediate filament protein (*NESTIN*), aniridia type II protein (*PAX6*), and *SRY*-box 1 (*SOX1*) (Fig. 1, M to P). Comparable neural precursor morphology in previously frozen and replated NPCs (passage 24) was also seen (fig. S2, A and B). Karyotype analysis using Giemsa banding (G-banding) demonstrated a stable karyotype in proliferating NPCs at passages 15 and 30 (fig. S2, C and D). Quantitative flow cytometry analysis showed $91 \pm 14\%$ of *SOX1*⁺ cells, $51.7 \pm 12\%$ of *PAX6*⁺, $90.8 \pm 9\%$ of *SOX2*⁺, and $72.3 \pm 17\%$ of *NESTIN*⁺ cells, respectively (fig. S2, E to J).

To characterize the multilineage potential of our iPSC-NPCs, we subcultured NPCs on an established human fetal astrocyte monolayer and then induced by withdrawal of bFGF and addition of cyclic adenosine monophosphate (cAMP), brain-derived neurotrophic factor (BDNF), and glial cell-derived neurotrophic factor (GDNF). The cultured NPCs were designed to express EGFP under the synapsin (*SYN*) promoter, and immunofluorescence staining of 8 week-induced NPCs showed multipolar EGFP⁺ neurons expressing doublecortin

(*DCX*) and Fox-3 (*NeuN*) (Fig. 1, Q and R). A subpopulation of *DCX*⁺ neurons showed γ -aminobutyric acid (GABA) immunoreactivity (Fig. 1S). *TUJ1* immunoreactivity was also seen (Fig. 1T). To assess the functionality of induced neurons in vitro, we measured spontaneous oscillation in cytosolic calcium (Ca^{2+}) after loading the induced neurons with the Ca^{2+} indicator dye Fluo-4 AM. A consistent cyclical type of calcium oscillation lasting between 4.0 and 17.6 s, suggestive of neuronal depolarization, was observed in numerous neurons (Fig. 1U, white boxed regions). To characterize quantitatively the number of neuronal and glial cells that can be induced from iPSC-NPCs, we treated proliferating NPCs with 1% porcine serum for 20 days. Qualitative and quantitative analyses of induced NPCs showed effective differentiation to neurons (expressing the neuronal marker *TUJ1*), astrocytes [expressing the astrocyte marker glial fibrillary acidic protein (GFAP)], and glial and oligodendrocytes/precursors [expressing *VIMENTIN*, chondroitin sulphate proteoglycan 4 (*NG2*), and oligodendrocyte transcription factor (*OLIG2*)] (fig. S2, K to N).

In vivo-transplanted iPSC-NPCs generate functional neurons at 7 to 10 months after grafting into striata of immunodeficient rats

We next tested the functionality of porcine iPSC-NPCs (*SYN*-EGFP-NPCs) after grafting into the striatum of adult immunodeficient rats (Fig. 2A). Animals ($n = 12$) received three bilateral injections of *SYN*-EGFP-NPCs (30,000 cells per injection; 2 μ l per injection site) into the striatum. One to 10 months after cell grafting, we prepared ex vivo brain slices and performed patch-clamp recordings from *SYN*-EGFP⁺ grafted cells (Fig. 2B and fig. S3A). A subset ($n = 6$) of grafted animals was perfused with cold saline, and striata were harvested for mRNA sequencing (to analyze porcine-specific transcripts) ($n = 2$; two individual NPC-grafted striata analyzed at 10 months after grafting) or fixed with 4% paraformaldehyde ($n = 4$; 7 months after grafting) and the grafted cells studied with immunofluorescence staining with neuron-specific antibodies [*NeuN*, neuron-specific enolase (*NSE*), *DCX*, *SYN*, vesicular GABA transporter (*VGAT*), gephyrin, and neurofilament (*NF*)]. A relative number (% of total EGFP⁺ neurons) of double-immunoreactive EGFP/*DCX*, EGFP/*NeuN*, and EGFP/*NSE* neurons was quantified using confocal microscope (table S1).

Patch-clamp recording in EGFP⁺ neurons showed that all the examined transplanted cells ($n = 3$) showed properties of mature neurons, such as robust trains of action potentials (average = 18 Hz) in response to 500-ms depolarizing steps of currents (Fig. 2C), large voltage-gated sodium/potassium currents (Nav peak average = -5745 pA) (Fig. 2D), low resting membrane potentials (average = -78 mV), and spontaneous excitatory synaptic activity (table S2).

Immunofluorescence staining revealed numerous *SYN*-EGFP⁺ neurons with extensive processes in the grafted striatal regions (Fig. 2E). Confocal microscopy showed that virtually all *SYN*-EGFP⁺ cells colocalized with *NeuN* (Fig. 2E, insets, and fig. S3, A and B). Similarly, intense porcine-specific, *NSE* expression (13) was seen in EGFP⁺ grafts (Fig. 2F and fig. S3C). Staining with antibodies specific for *SYN* and/or *VGAT* showed a high density of *SYN*/EGFP⁺ or *SYN*/*VGAT*⁺ puncta on the soma/membranes of endogenous *NeuN*-positive neurons or EGFP⁺ grafted neurons (Fig. 2, G and H, and fig. S3D). Costaining with presynaptic inhibitory marker (*VGAT*) and postsynaptic glycine receptor marker (gephyrin) showed the presence of glycine receptors on grafted EGFP⁺ neurons in opposition to *VGAT*⁺ terminals (Fig. 2I, inset), suggesting the development of inhibitory glycinergic synaptic contacts.

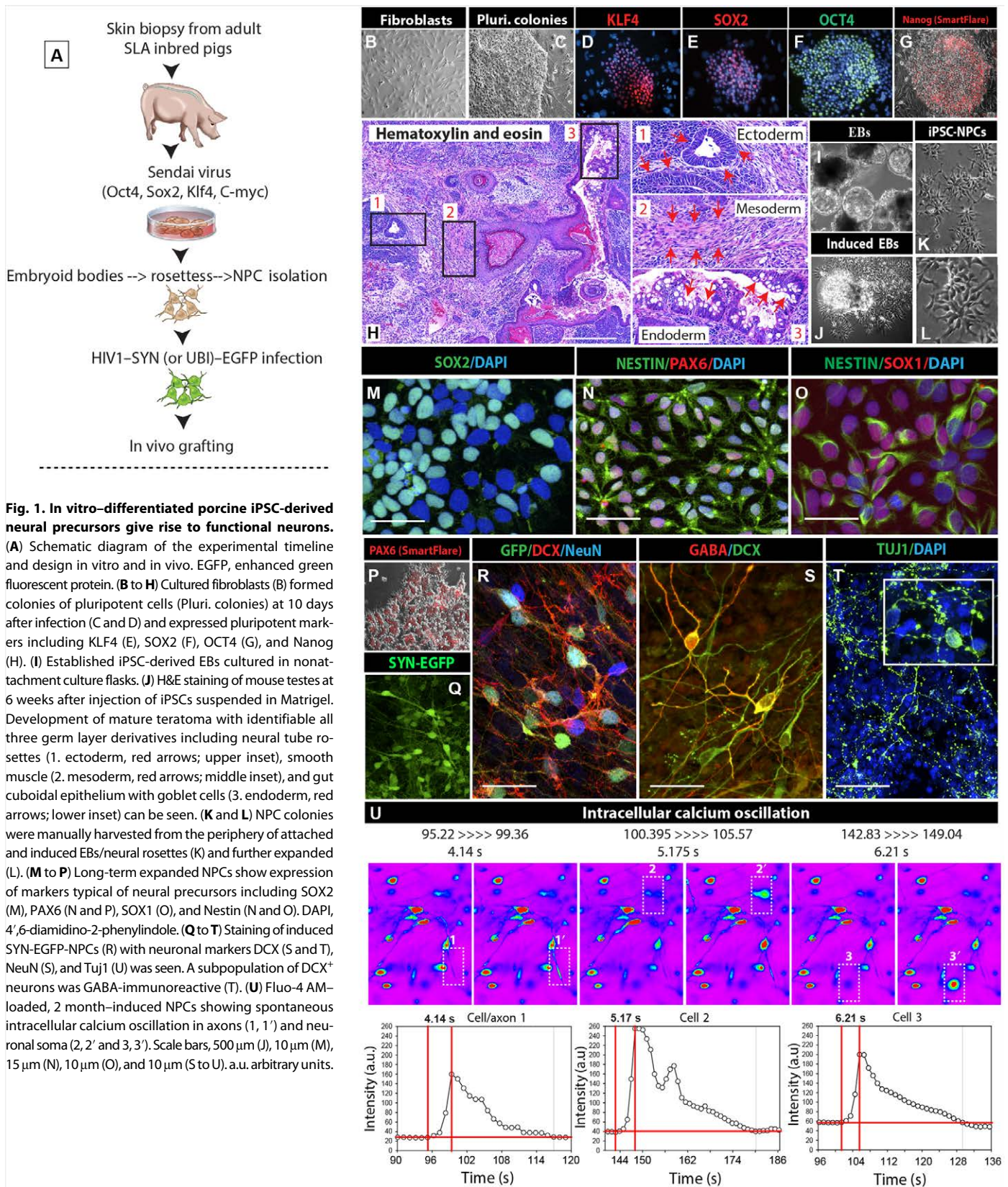


Fig. 1. In vitro-differentiated porcine iPSC-derived neural precursors give rise to functional neurons. (A) Schematic diagram of the experimental timeline and design in vitro and in vivo. EGFP, enhanced green fluorescent protein. (B to H) Cultured fibroblasts (B) formed colonies of pluripotent cells (Pluri. colonies) at 10 days after infection (C and D) and expressed pluripotent markers including KLF4 (E), SOX2 (F), OCT4 (G), and Nanog (H). (I) Established iPSC-derived EBs cultured in nonattachment culture flasks. (J) H&E staining of mouse testes at 6 weeks after injection of iPSCs suspended in Matrigel. Development of mature teratoma with identifiable all three germ layer derivatives including neural tube rosettes (1. ectoderm, red arrows; upper inset), smooth muscle (2. mesoderm, red arrows; middle inset), and gut cuboidal epithelium with goblet cells (3. endoderm, red arrows; lower inset) can be seen. (K and L) NPC colonies were manually harvested from the periphery of attached and induced EBs/neural rosettes (K) and further expanded (L). (M to P) Long-term expanded NPCs show expression of markers typical of neural precursors including SOX2 (M), PAX6 (N and P), SOX1 (O), and Nestin (N and O). DAPI, 4',6-diamidino-2-phenylindole. (Q to T) Staining of induced SYN-EGFP-NPCs (R) with neuronal markers DCX (S and T), NeuN (S), and Tuj1 (U) was seen. A subpopulation of DCX⁺ neurons was GABA-immunoreactive (T). (U) Fluo-4 AM-loaded, 2 month-induced NPCs showing spontaneous intracellular calcium oscillation in axons (1, 1') and neuronal soma (2, 2' and 3, 3'). Scale bars, 500 μ m (J), 10 μ m (M), 15 μ m (N), 10 μ m (O), and 10 μ m (S to U). a.u. arbitrary units.

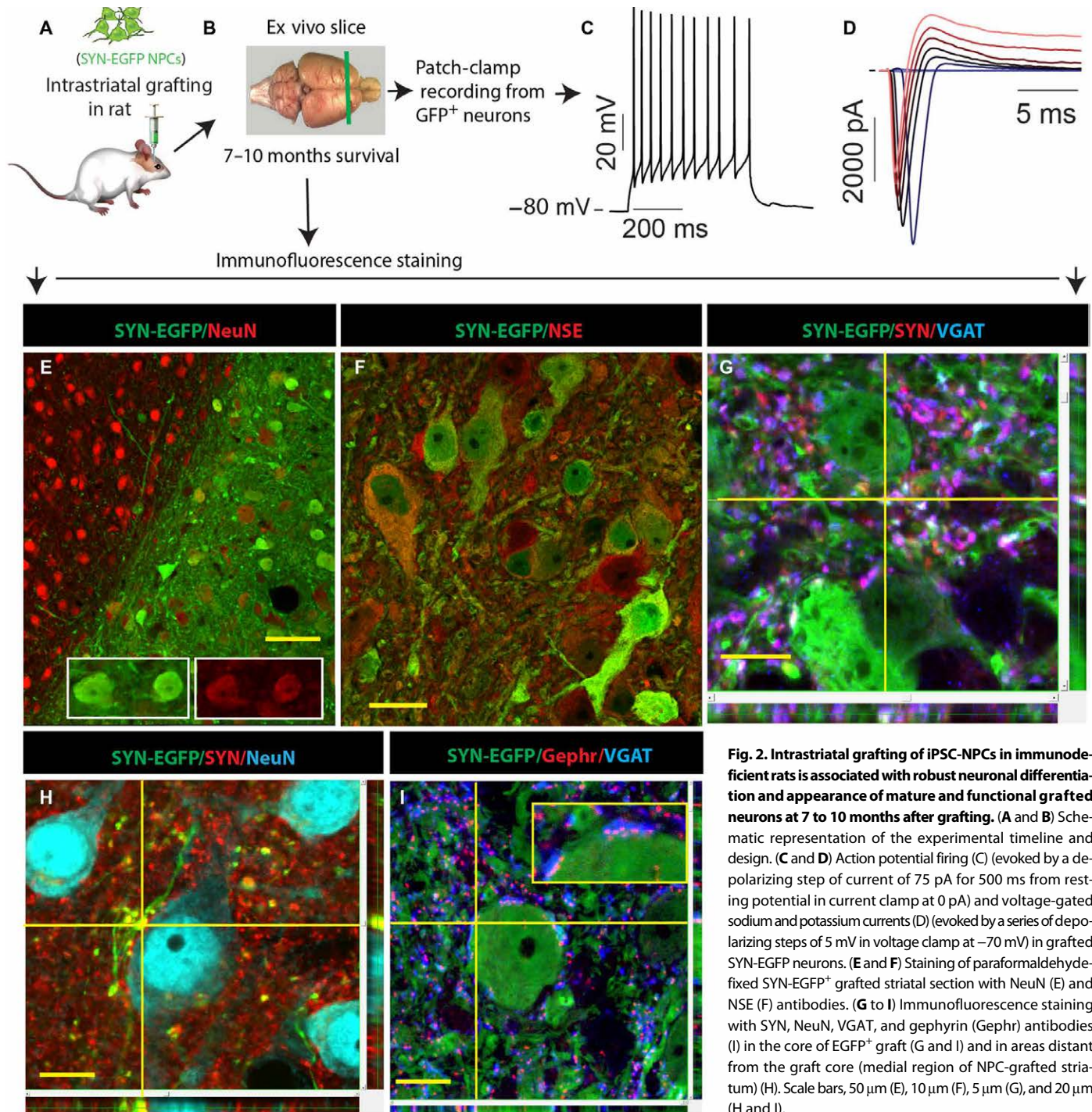


Fig. 2. Intrastratial grafting of iPSC-NPCs in immunodeficient rats is associated with robust neuronal differentiation and appearance of mature and functional grafted neurons at 7 to 10 months after grafting. (A and B) Schematic representation of the experimental timeline and design. (C and D) Action potential firing (C) (evoked by a depolarizing step of current of 75 pA for 500 ms from resting potential in current clamp at 0 pA) and voltage-gated sodium and potassium currents (D) (evoked by a series of depolarizing steps of 5 mV in voltage clamp at -70 mV) in grafted SYN-EGFP neurons. (E and F) Staining of paraformaldehyde-fixed SYN-EGFP⁺ grafted striatal section with NeuN (E) and NSE (F) antibodies. (G to I) Immunofluorescence staining with SYN, NeuN, VGAT, and gephyrin (Gephr) antibodies (I) in the core of EGFP⁺ graft (G and I) and in areas distant from the graft core (medial region of NPC-grafted striatum) (H). Scale bars, 50 μ m (E), 10 μ m (F), 5 μ m (G), and 20 μ m (H and I).

Staining with NF antibody showed high-density NF neural processes within EGFP⁺ grafts (fig. S3E).

Transplanted iPSC-NPCs are nontumorigenic and acquire genetic signature of mature porcine CNS at 7 to 10 months after grafting into striata of immunodeficient rats

We next performed whole-transcriptome mRNA-sequencing analysis on the striatum of immunodeficient rats that had received iPSC-

NPC grafts (Fig. 3, A to D). Striatal tissue was harvested 10 months after iPSC-NPC grafting. To separate the pig mRNA sequence reads from the host rat mRNA reads, we developed a bioinformatics pipeline to sort mRNA sequence reads in a species-specific manner to either pigs or rats (Fig. 3E). Slight variations in the genome sequence between pigs and rats allowed us to differentiate between the species with a high sensitivity (99.52% efficiency). We detected 9332 pig genes expressed in the grafted rat striatum. This represented 5.19%

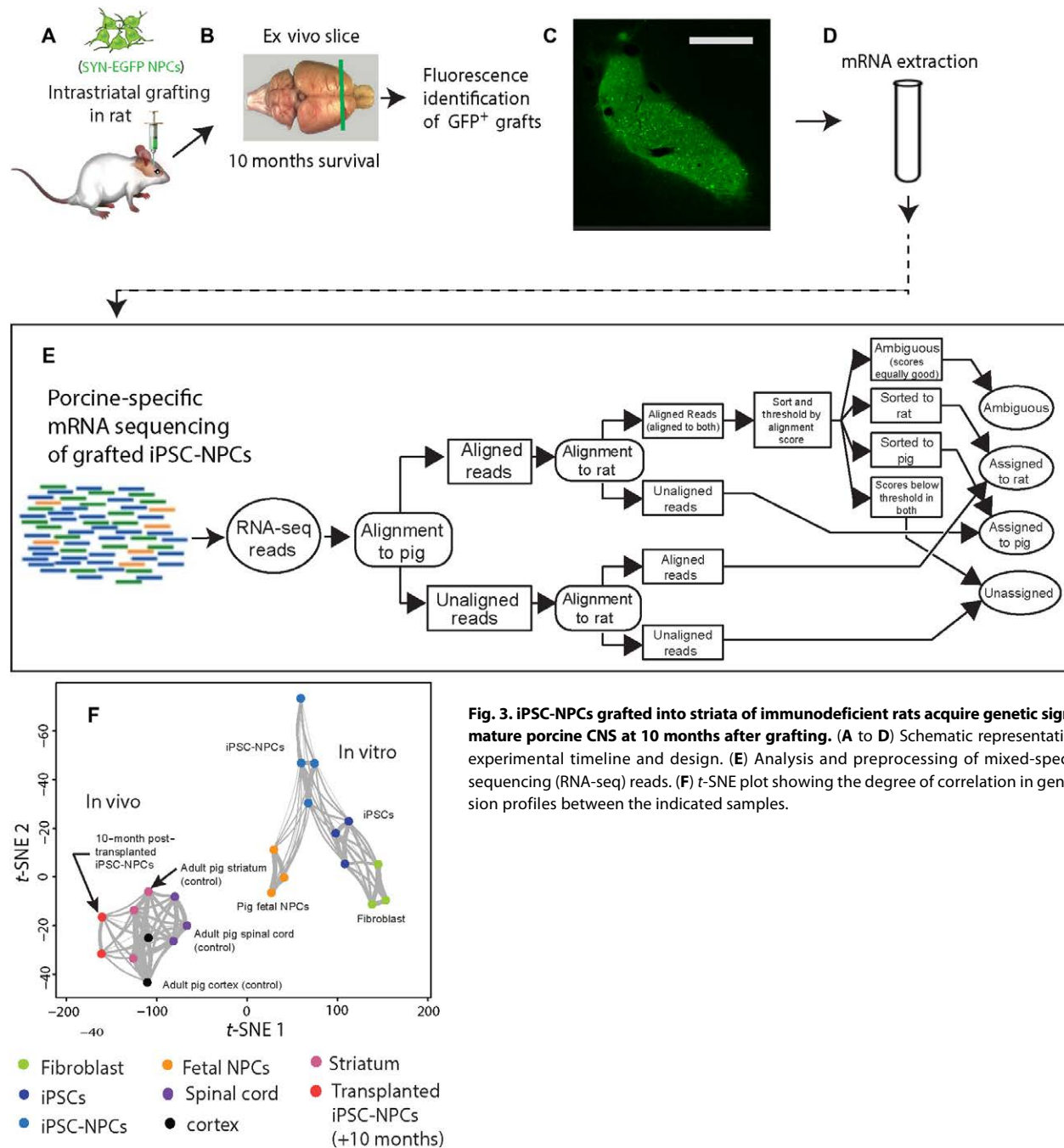


Fig. 3. iPSC-NPCs grafted into striata of immunodeficient rats acquire genetic signature of mature porcine CNS at 10 months after grafting. (A to D) Schematic representation of the experimental timeline and design. (E) Analysis and preprocessing of mixed-species RNA-sequencing (RNA-seq) reads. (F) *t*-SNE plot showing the degree of correlation in gene expression profiles between the indicated samples.

of the total mRNA reads from the graft tissue, with a false-positive sorting rate of 0.47% (appendix S1 and table S3). Gene expression was analyzed with *t*-distributed stochastic neighbor embedding (*t*-SNE) to determine the global gene expression patterns in the samples. Gene expression patterns from the transplanted iPSC-NPCs correlated strongly with the expression pattern of control mature pig CNS tissue, but not with the original iPSC-NPCs or iPSC populations (Fig. 3F). Analysis of mature CNS-specific transcripts in grafted cells shows high expression of neuronal markers and only moderate to low expression of glial genes (fig. S3, F and G). These data indicate that transplanted iPSC-NPCs differentiate normally into neuronal and glial

subtypes and adopt gene expression patterns indicative of the environment into which they were grafted.

To identify any neuropathologically defined signs of tumor formation, we also stained sections using H&E. Consistent with immunofluorescence staining, well-incorporated grafts that fused with the host tissue were identified. No gross signs of tissue necrosis or aberrant tissue proliferation were noted (fig. S4A). Staining with myelin basic protein (MBP) and OLIG2 antibodies showed incomplete myelination in EGFP⁺ grafts, which was in contrast with the surrounding host tissue (fig. S4, B to D). In the same areas, the presence of VIMENTIN⁺ cells and oligodendrocytes (OLIG2⁺) was also seen, suggesting ongoing myelination (fig. S4, E to G).

Staining with endothelial marker Recla-1 showed regularly distributed vessel profiles in EGFP⁺ grafts (fig. S5, A and B). The expression of a subset of proto-oncogenes and tumor suppressor genes in grafted rat striata at 10 months after grafting was very similar to that observed in normal control pig spinal cord and striatum tissue (fig. S5C).

Collectively, these data show that we have generated a transplantable, nontumorigenic population of porcine iPSC-NPCs that shows a robust neuronal differentiation and is functional once grafted into the adult CNS of immunodeficient rats.

Syngeneic porcine iPSC-NPCs grafted spinally in adult naïve pigs show long-term survival in the absence of immunosuppression

We next tested whether the syngeneic transplantation of porcine iPSC-NPCs into the lumbar spinal cord of naïve spinally noninjured pigs would support cell survival in the absence of immunosuppression. Three SLA fully matched minipigs received 20 bilateral syngeneic grafts of iPSC-NPCs (SYN-EGFP⁺) targeted into the central gray matter of the L2–L5 spinal cord segments (50,000 live cells/ μ l, 10 μ l per injection). Three months after grafting, the animals were sacrificed and the spinal cord was harvested for subsequent analysis.

Immunofluorescence analysis of horizontal spinal cord sections throughout the grafted region showed the presence of long bilateral EGFP⁺ grafts extending for more than 2 cm (Fig. 4A and fig. S6A). No tumor formation or aberrant tissue mass was seen in any animal. High-density NF-positive and GFAP-positive networks were identified in EGFP⁺ grafts (Fig. 4, B and C, and fig. S6, B and C). Staining with neuron-specific markers including DCX, NeuN, and NSE showed neurons that occupied the entire EGFP⁺ grafts (Fig. 4, D to F, and fig. S6, D to F). Analysis of axonal projections into regions caudal and cranial from the border of the EGFP⁺ graft showed the projection of EGFP⁺ axons for distances longer than 2 to 3 cm. These axons showed coexpression of NF (Fig. 4, G to I). A quantitative analysis (% of total EGFP⁺ neurons) of double-immunoreactive EGFP/DCX, EGFP/NeuN, and EGFP/NSE neurons is presented in table S1.

Staining with the SYN antibody revealed a high density of SYN⁺ puncta throughout the EGFP⁺ graft (fig. S6G). The majority of the EGFP/SYN⁺ puncta displayed colocalization with VGAT and was opposed to postsynaptic gephyrin⁺ puncta found on EGFP⁺ grafted neurons or EGFP-negative host neurons (Fig. 4, J and K, and fig. S6G). These data demonstrate the development of putative inhibitory synaptic contacts.

Syngeneic pigs receiving spinal iPSC-NPCs grafts show no humoral immunity against grafted cells at 3 months after cell transplantation

To test for the presence of circulating anti-iPSC-NPC antibodies in syngeneic pigs grafted spinally with iPSC-NPCs, a combined *in vivo* and *ex vivo* immunostaining assay was developed. First, a homogenate mixture composed of proliferating or induced iPSC-NPCs (in Freund's adjuvant; non-EGFP-tagged cells) was injected subcutaneously to immunize an allogeneic pig (Fig. 5A). In parallel, the same NPC population (but expressing EGFP under SYN promoter) was injected into the striata or lumbar spinal cord in immunodeficient rats. Six months after grafting, rat brain and spinal cord sections containing iPSC-NPC-EGFP were harvested and stained using the sera taken from immunized pig (positive control), naïve nonimmunized allogeneic pig (negative control), and syngeneic pigs that had previously received spinal iPSC-NPC-EGFP grafts.

Staining of rat striatal and spinal cord sections (harvested at 6 months after grafting) containing iPSC-NPC-EGFP⁺ grafts with pig sera from immunized pigs showed cellular staining in grafted EGFP⁺ neurons (positive control, Fig. 5B). No staining was observed with sera taken from nonimmunized pigs (negative control) or from a syngeneic pig grafted spinally with iPSC-NPC-EGFP (Fig. 5, C and D). These data demonstrate that no humoral immune reaction developed in syngeneic pig for a minimum of 3 months after cell grafting.

Short-term immunosuppression (4 weeks) induces immune tolerance to allogeneic iPSC-NPCs grafted spinally in adult pigs with previous chronic spinal traumatic injury

We next tested whether porcine iPSC-NPCs (the same cell line as that used for syngeneic spinal grafting) could survive and differentiate after transplantation into the lumbar spinal cord of allogeneic pigs in the context of both spinal cord injury and transient (1 month) immunosuppression. Allogeneic minipigs ($n = 3$) that had undergone a spinal cord injury in the L3 segment received 20 bilateral grafts of iPSC-NPC-EGFP [under ubiquitin (UBI) promoter; 50,000 live cells/ μ l, 10 μ l per injection] 2.5 months after spinal trauma. After cell grafting, animals were immunosuppressed for 4 weeks with Prograf (0.025 mg/kg per day, intravenously). After an additional 2.5 months without immunosuppression, the presence of grafted cells was analyzed in spinal cord sections using immunofluorescence (Fig. 6A). The relative number (% of total EGFP⁺ neurons, astrocytes, and oligodendrocytes) of double-immunoreactive EGFP/DCX, EGFP/NeuN, and EGFP/NSE neurons and EGFP/GFAP and EGFP/OLIG2 glial cells was quantified using four sections per animal containing a clearly identifiable EGFP⁺ graft. The degree of SLA mismatch between the iPSC-NPC donor and graft recipients was analyzed in skin fibroblast DNA extracts using polymerase chain reaction–based SLA genotyping assays (14, 15).

The injured spinal cord regions were found to be extensively populated by grafted NPC-EGFP⁺ cells in all three animals. The length of individual fused grafts ranged between 2 and 3 cm (Fig. 6, B and C, and fig. S7A). Staining with NeuN antibody showed NeuN⁺ neurons throughout the EGFP⁺ grafts (Fig. 6, B and D to F). A high density of SYN expression in EGFP⁺ grafts was also observed and was similar to that seen in the surrounding host tissue (Fig. 6B; top right inset). Costaining with NeuN and NF antibodies showed high-density NF⁺ neurites in NeuN-populated grafts (Fig. 6G). Staining with DCX and NSE antibodies showed numerous DCX/NSE-expressing EGFP⁺ neurons at different stages of neuronal maturation (Fig. 6H and fig. S7, B to E). Triple staining with SYN, EGFP, and VGAT antibodies confirmed a high density of SYN/VGAT terminals associated with EGFP puncta (Fig. 6I and fig. S7F). EGFP/SYN/VGAT⁺ puncta were opposed to postsynaptic gephyrin⁺ puncta seen on EGFP⁺ grafted neurons or EGFP-negative host neurons (Fig. 6J and fig. S7G). Staining with postsynaptic excitatory marker Homer 1 (postsynaptic protein associated with group 1 metabotropic glutamate receptor) showed a clear punctate-like staining on neuronal soma and axons of EGFP⁺ grafted neurons (Fig. 6K and fig. S7H).

Staining with GFAP and OLIG2 antibodies revealed graft-derived astrocytes and oligodendrocytes (Fig. 6, L to N, and fig. S7I). Costaining with choline acetyltransferase (CHAT) antibody showed the occasional presence of CHAT⁺ neurons (fig. S7J). Detailed regional analysis of NeuN expression in UBI-EGFP–grafted regions showed homogeneous distribution of NeuN⁺ neurons through the whole engrafted region (fig. S8, A to D). A quantitative analysis (% of total EGFP⁺ neurons)

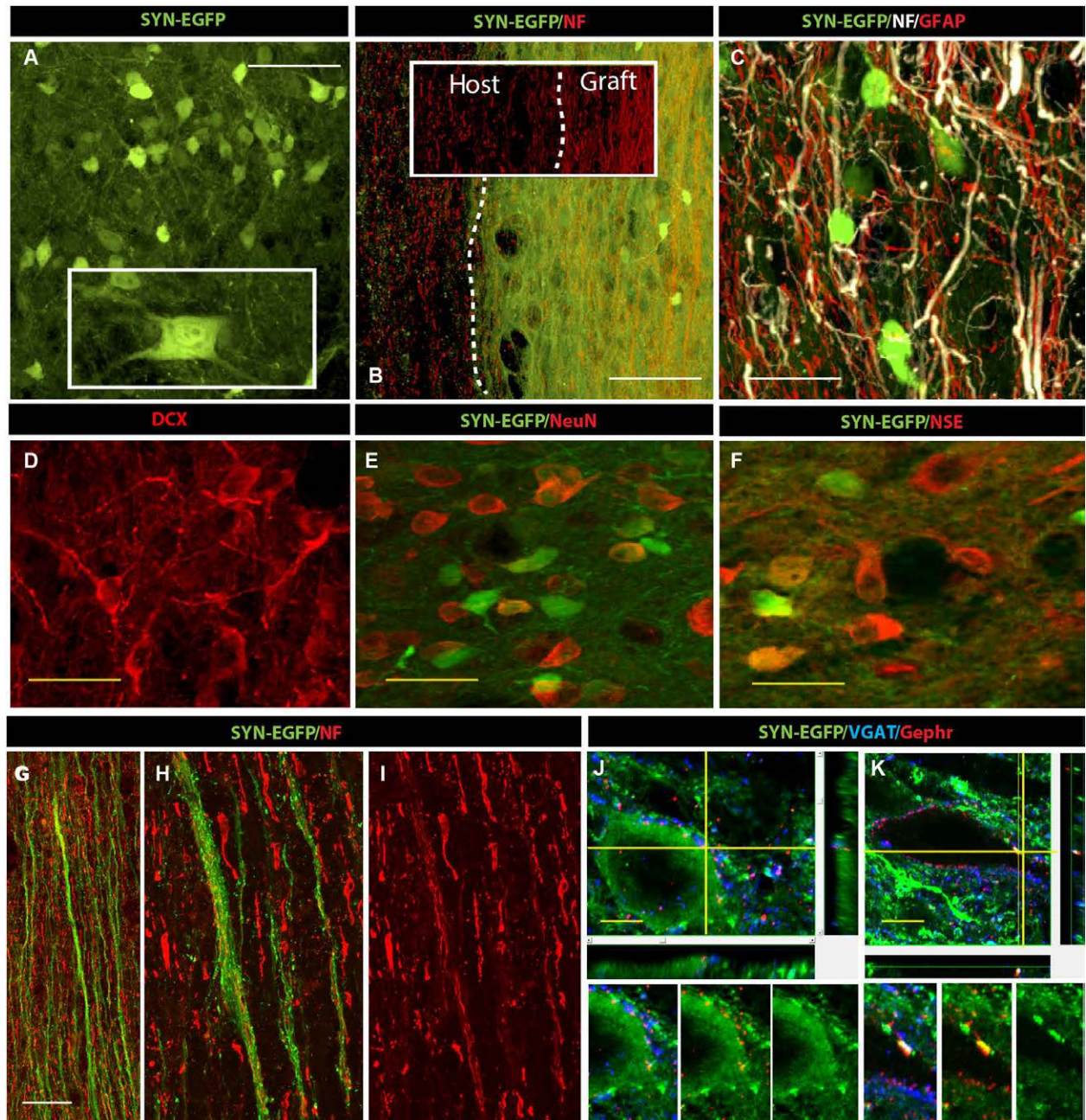


Fig. 4. Spinally grafted iPSC-NPCs show long-term survival and neuronal and glial differentiation in syngeneic recipient in the absence of immunosuppression. (A) Immunofluorescence staining showing EGFP fluorescence in the core of the graft. (B and C) Immunofluorescence staining showing NF- and GFAP-stained processes in the same areas as in (A). (D to F) Staining with DCX (D), NeuN (E), and NSE (F) in EGFP⁺ grafts. (G to I) Immunofluorescence staining showing EGFP/NF⁺ neurites, in areas cranial and caudal to the borders of the graft. (J and K) Costaining of SYN-EGFP⁺ grafts with VGAT and gephyrin antibodies in the core of the graft. Scale bars, 30 μm (A), 125 μm (B), 10 μm (C), 40 μm (D), 35 μm (E and F), 50 μm (G to I), and 20 μm (J and K).

of double-immunoreactive EGFP/DCX, EGFP/NeuN, EGFP/NSE, EGFP/GFAP, and EGFP/OLIG2 neurons and glial cells is presented in table S1.

The H&E staining showed well-incorporated individual grafts with morphology consistent with mature neural tissue (fig. S9A). In comparison with the host surrounding tissue, incomplete myelination was observed, as evidenced by a low density of MBP immunoreactivity within EGFP⁺ grafts (fig. S9, B and C). Numerous triple-stained

EGFP/VIMENTIN/Ki67⁺ cells were found within EGFP⁺ grafts [fig. S9, D (insets) and E]. These data suggest ongoing myelination and proliferation of glial precursors. To study the dynamics of cell proliferation (Ki67⁺ cells) in developing porcine spinal cord, we next stained spinal cord sections prepared from 70-day-old porcine fetus (gestational period in pig is around 115 days), newborn piglet, and adult naïve pig (18 months old). In the 70-day-old fetus, a high density of Ki67⁺ cells in both white and gray matter regions was seen.

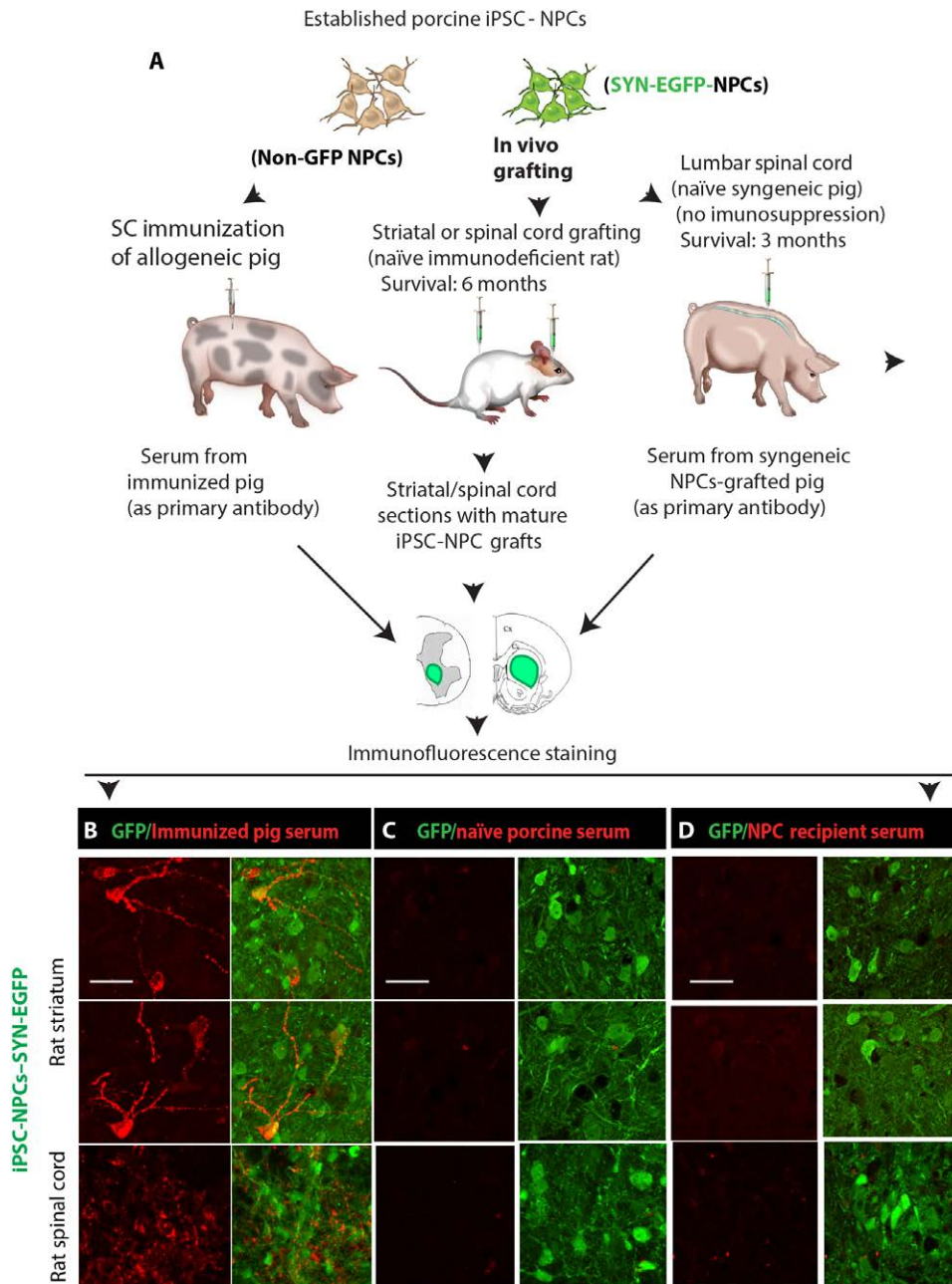


Fig. 5. Syngeneic iPSC-NPC recipients show no humoral immunity against grafted cells at 3 months after cell transplantation in the absence of immunosuppression. (A) Schematic diagram of the development of in vivo/ex vivo staining protocol to detect the presence of circulating antibodies against grafted iPSC-NPCs. (B to D) Staining of mature iPSC-NPC grafts in rat striatum and rat spinal cord with serum from previously anti-iPSC-NPC-immunized pig (B), sera harvested from naïve nonimmunized pig (C), or with sera from syngeneic iPSC-NPC-grafted pigs ($n = 3$) (D) 3 months after grafting. Scale bars, 40 μm (B to D).

The number of Ki67⁺ cells decreased in newborn piglets but was still present in the adult pig (fig. S9, F to I). These data are consistent with a previous report in mice that demonstrated an ongoing proliferation of glial precursors in the intact adult spinal cord (16).

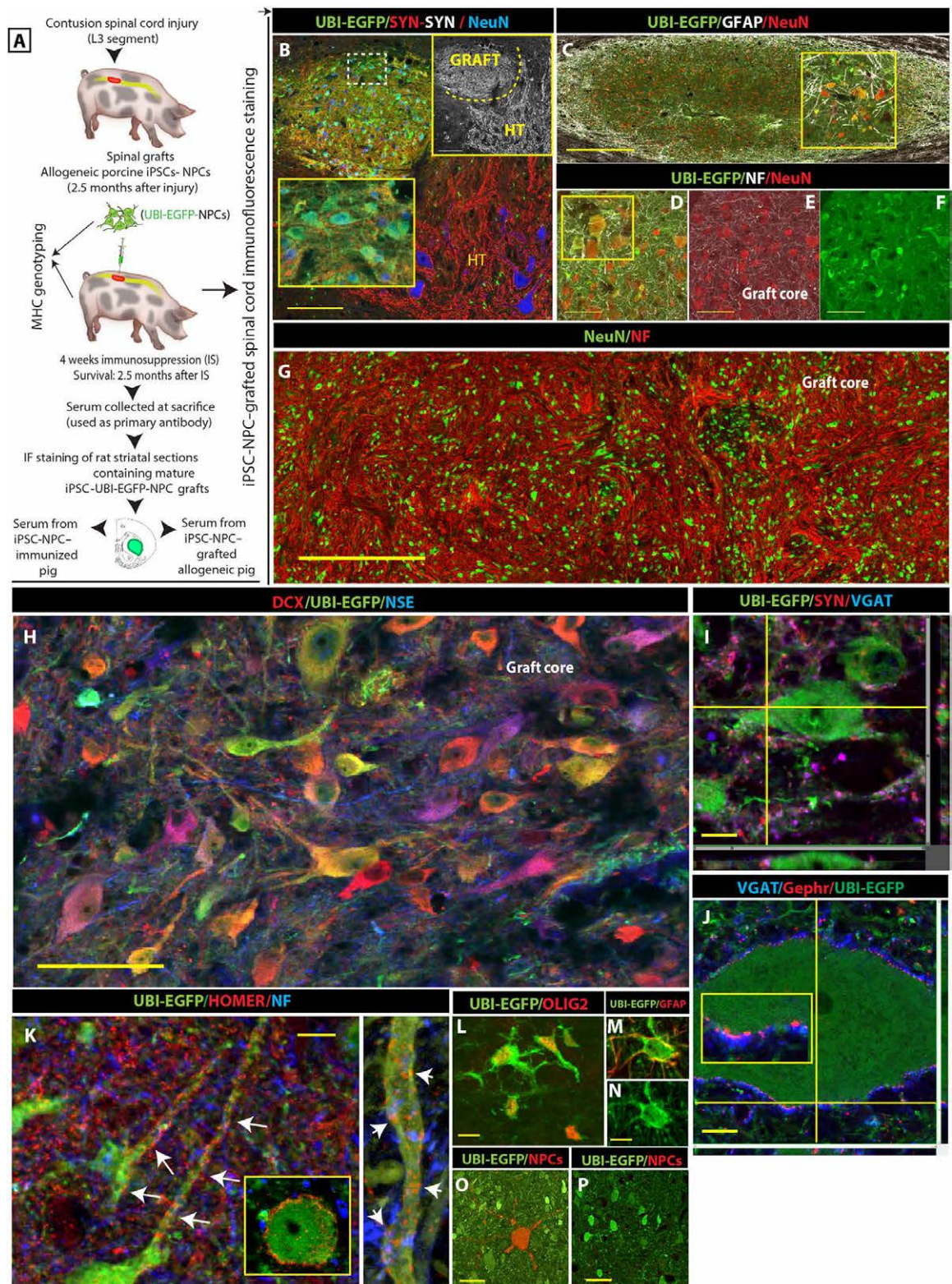
Transiently immunosuppressed (4 weeks) allogeneic, spinally injured pigs show no humoral or cellular immunity against grafted iPSC-NPCs at 2.5 months after cell transplantation

in syngeneic pigs and more diffuse presence of CD45/CD8-positive cells in allogeneic spinally injured pigs with continuous or transient immunosuppression (Fig. 7, G to I). Analysis of double MHC-II- and Iba1-stained sections showed that virtually all MHC-II⁺ cells expressed Iba1 (Fig. 7J). Quantitative comparative analysis of CD45- and CD8-positive cells between allogeneic spinally injured continuously immunosuppressed animals (1-month postgrafting survival)

Next, we tested the presence of circulating antibodies against iPSC-NPCs by staining mature (6 months after grafting) iPSC-NPC grafts in the rat striata with sera harvested from allogeneic iPSC-NPC-grafted pigs. In contrast to the strong staining observed with sera from anti-iPSC-NPC-immunized pig, no staining was detected with sera from allogeneic graft recipients (Fig. 6, O and P). As shown in table S4 (A and B), the SLA genotypes of the iPSC-NPC donor and the allogeneic graft recipients were well mismatched at both the antigen (allele group) and allele level across the class I (*SLA-1*, *SLA-2*, and *SLA-3*) and class II (*DRB1*, *DQA*, and *DQB1*) loci tested (17–23).

To further probe for the presence of an immune response in cell-grafted spinal cord regions, we stained spinal sections with porcine-specific anti-major histocompatibility complex II (MHC-II), CD45 (leukocyte common antigen), CD8 (co-receptor for the T cell receptor), and ionized calcium-binding adapter molecule 1 (Iba1; microglial marker) antibodies. Sections were taken from the following: (i) spinal cord of syngeneic pigs 3 months after iPSC-NPC grafting without immunosuppression; (ii) spinal cord of injured, continuously immunosuppressed allogeneic pigs 4 weeks after iPSC-NPC grafting; and (iii) spinal cord of injured, transiently immunosuppressed allogeneic pigs 3.5 months after iPSC-NPC grafting. In syngeneic pigs, the staining with anti-MHC-II antibody showed that the immunoreactivity was restricted around the needle injection tracts (Fig. 7A). In allogeneic spinally injured animals with continuous or transient immunosuppression, a more diffuse staining pattern was seen, and MHC-II⁺ cells were observed throughout the EGFP⁺ graft as well as in surrounding injured host tissue (Fig. 7, B and C). Staining with Iba1 antibody exhibited a very similar staining pattern as was seen for MHC-II staining (Fig. 7, D to F). Staining with CD45 and CD8 antibodies showed accumulation of both cell types around the cell injection tract

Fig. 6. Spinally grafted iPSC-NPCs show long-term survival and neuronal and glial differentiation in allogeneic spinally injured pigs with transient immunosuppression. (A) Schematic diagram of experimental design. IF, immunofluorescence. (B to F) Costaining of EGFP⁺ grafts with NeuN, synaptophysin, and GFAP antibodies. HT, host tissue. (G) Costaining with NF and NeuN antibodies in the core of the graft. (H) Costaining of DCX, EGFP, and NSE in the core of the graft. (I) Confocal microscopy image of SYN and VGAT puncta on EGFP⁺ grafted neurons. (J) Staining of EGFP⁺ grafted neuron with VGAT and gephyrin antibodies. (K) Costaining with HOMER and NF antibodies of EGFP⁺ grafted neurons (white arrows indicate HOMER⁺ puncta on neuronal soma or axons of EGFP⁺ neurons). (L to N) Confocal images of double-labeled EGFP⁺/OLIG2⁺ oligodendrocytes and EGFP⁺/GFAP⁺ astrocytes. (O and P) Staining of mature iPSC-NPC-EGFP⁺ grafts in rat striata with sera from anti-iPSC-NPC-immunized pigs (O) or with sera from iPSC-NPC-grafted transiently immunosuppressed allogeneic pig (*n* = 3) (P). Scale bars, 300 μ m (B), 500 μ m (C), 60 μ m (D to F), 250 μ m (G), 60 μ m (H), 10 μ m (I), 5 μ m (J), 10 μ m (K), 10 μ m (L and N), and 40 μ m (O and P).



and animals with transient immunosuppression 3 months after grafting showed a significant decrease in the number of both CD45⁺ and CD8⁺ cells 3 months after cell grafting in transiently immunosuppressed animals (Fig. 7, K and L).

These data demonstrate that spinal grafting of iPSC-NPCs in syngeneic nonimmunosuppressed or allogeneic transiently immunosuppressed animals leads to a robust graft survival with minimal immune response at the site of cell grafting.

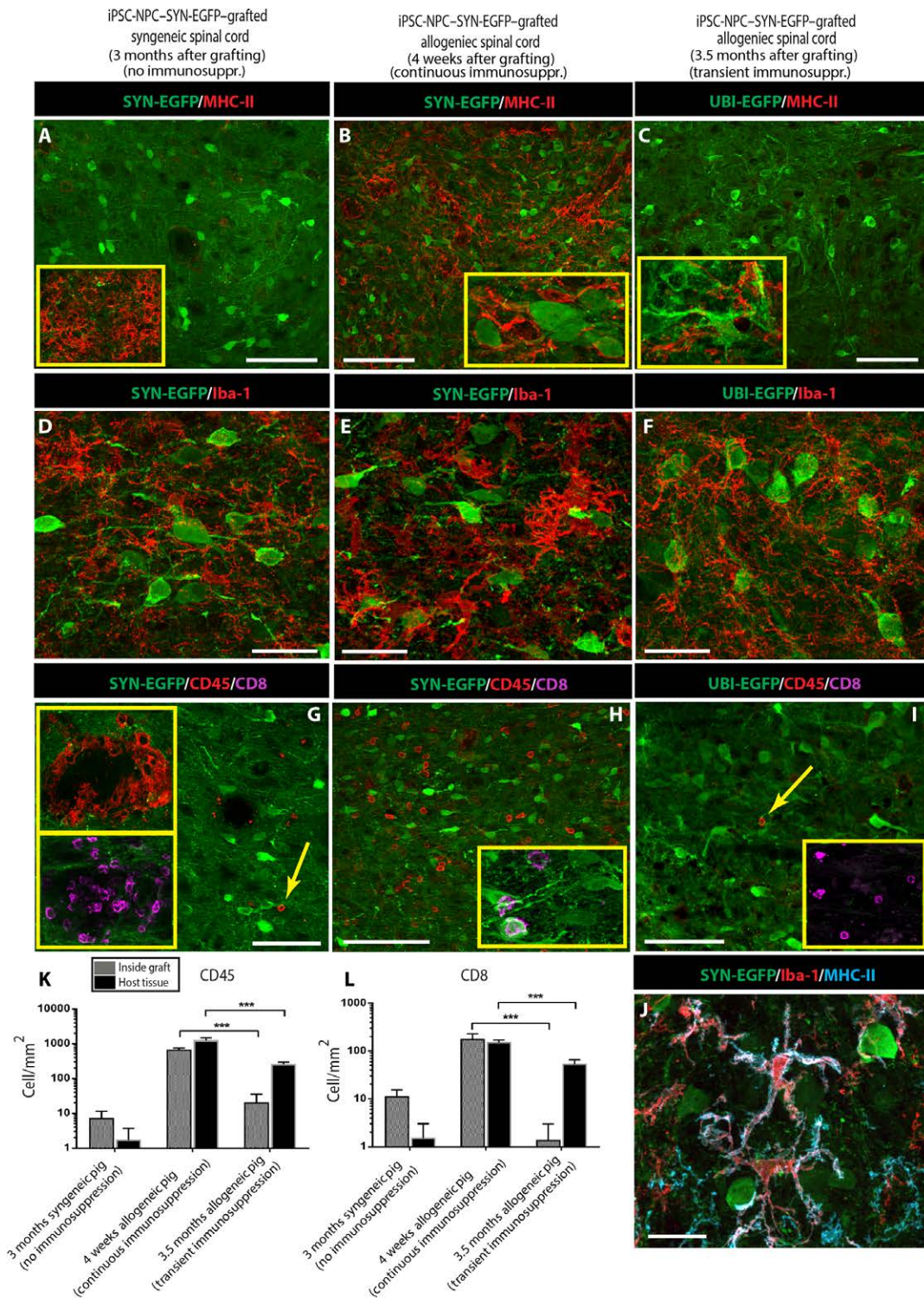


Fig. 7. Transient immunosuppression (4 weeks) supports long-term graft survival and is associated with progressive decrease in spinal regional inflammatory response in iPSC-NPC-grafted spinally injured allogeneic pig. (A to C) Immunofluorescence staining for MHC-II and EGFP around cell injection needle tract in syngeneic pigs (A; $n = 3$) and in allogeneic continuously immunosuppressed (B; $n = 3$) or transiently immunosuppressed (C; $n = 3$) spinally injured pigs 4 weeks or 3.5 months after cell grafting. (D to F) Immunofluorescence staining for Iba1 and EGFP around cell injection needle tract in syngeneic pigs (D) and in allogeneic continuously immunosuppressed (E) or transiently immunosuppressed (F) spinally injured pigs 4 weeks or 3.5 months after cell grafting. (G to I) Immunofluorescence staining for CD45, CD8, and EGFP around cell injection needle tract in syngeneic pigs (G) and in allogeneic continuously immunosuppressed (H) or transiently immunosuppressed (I) spinally injured pigs 4 weeks or 3.5 months after cell grafting. (J) Colocalization of MHC-II with Iba1 in the core of the graft. (K and L) Quantitative analysis of CD45⁺ and CD8⁺ leukocytes in EGFP⁺ grafts and in surrounding host tissue (Student's *t* test; *** $P < 0.05$). Scale bars, 300 μm (A to C and G to I), 20 μm (D to F), and 10 μm (J).

Analysis of neurological function in allogeneic NPC-grafted animals 3.5 months after grafting was performed using a previously developed porcine neurological scale designed to quantify the loss of motor function after spinal cord traumatic injury in adult pigs (24). Grade “0” corresponds with complete paraplegia with no detectable movement in the hindlimbs, and grade “14” corresponds with normal ambulatory function. NPC-grafted animals showed 2 to 3 degrees improvement (from grade 6 to grade 8 or 9) compared to pretransplantation baseline. This corresponds to better movement in all three joints of lower extremities but with no ability to support weight or walk.

Reprogramming factors and immunogenic genes are not expressed in vivo in grafted iPSC-NPCs

We next studied the residual protein expression of reprogramming factors (OCT4, KLF4, and SOX2) and Sendai virus-associated protein (SeV) in grafted cells at 3 and 7 months after grafting by using sections taken from grafted rat striata and allogeneic pig spinal cord. Sections were also stained with Ki67 antibody. Staining with OCT4 and KLF4 antibodies showed no residual staining in grafted cells (fig. S10, A to H). Staining with SOX2 antibody showed regularly distributed SOX2⁺ cells within EGFP⁺ grafts in both rat striata and allogeneic pig spinal cord (fig. S10, I to L). In allogeneic pig spinal cord, a specific SOX2 expression was also seen in endogenous ependymal cells of central canal (fig. S10L, white dotted line). Staining with Ki67 antibody showed regularly distributed double EGFP/Ki67-stained cells in both rat striata and allogeneic pig spinal cord grafts (fig. S10, M to P). Staining with anti-SeV antibody revealed only occasional presence of Sendai virus-associated protein in grafted EGFP⁺ cells (fig. S11, A to D). The mRNA-sequencing analysis showed no apparent differences in several immunogenic genes including *Hormad1* and *Cyp39A1* (fig. S11E).

DISCUSSION

Using nonintegrating Sendai virus (encoding *OCT4*, *SOX2*, *KLF4*, and *c-MYC*), we demonstrated the successful reprogramming of porcine skin fibroblasts harvested from adult fully SLA-matched pigs to iPSCs. After iPSC induction, we isolated the NPCs by manual selection and expanded for more than 20 passages while maintaining a stable karyotype and expressing markers typical of NPCs (such as *SOX1*, *SOX2*, *NESTIN*, and *PAX6*). Once grafted into the striata of immunodeficient rats or the spinal cord of syngeneic naïve noninjured pigs in the absence of immunosuppression, NPCs differentiated into functional neurons and glial cells (astrocytes and oligodendrocytes). Consistent with an advanced stage of grafted NPC maturation, the mRNA-sequencing analysis of porcine-specific transcripts in rat striata at 10 months after grafting showed a pattern of expression similar to control mature pig CNS tissue. Moreover, long-term survival of iPSC-NPC-derived cells was observed after grafting into spinal cord-injured allogeneic pigs that had received only transient immunosuppression.

A previous study has reported immunogenicity from syngeneic mouse iPSCs upon transplantation that may be related to an ongoing overexpression of pluripotent genes (25). In addition, several other factors such as expression of virus-related proteins generated by episomal vectors used for reprogramming and the MHC expression in specific iPSC derivatives may contribute to overall immunogenicity of transplanted cells (25). We have addressed those issues and have demonstrated that (i) there is no expression of pluripotent

genes at 3 to 7 months after transplantation and (ii) only occasional Sendai virus-associated protein was present in grafted iPSC-NPCs. These data suggest that, although a residual Sendai viral protein is present at the moment of grafting, it is not sufficient to trigger hyperacute or late T cell-mediated rejection. We have also demonstrated a lack of humoral or cellular response in syngeneic and allogeneic pigs receiving iPSC-NPC grafts. These data further demonstrate that even a mature iPSC-NPC graft does not express antigens that would be sufficient to initiate an immune response at prolonged periods after grafting.

In addition, there are several other variables that we believe need to be considered while generating iPSC-derived transplantable cell lines for experimental or clinical application. It has been demonstrated that several genes are expressed at abnormally high levels in mouse iPSCs. A subset of up-regulated genes with known immunogenic properties, including *Hormad1*, *Zg16*, and *Cyp3a11*, has been found to be directly linked to the T cell-mediated rejection of teratomas that formed after grafting of mouse iPSC lines into syngeneic recipients (25). All the iPSCs used in this previous study (13) came from fetal fibroblasts, an unlikely source for future therapies in humans, and the gene expression changes may be related to epigenetic memory of this specific developmental time. The use of adult fibroblast in our current experiments may contribute to the lack of immunogenic gene up-regulation.

Altered gene expression can also be due to the transcriptional memory observed in iPSCs (26, 27) or caused by somatic alterations in protein-coding regions accumulated in these cells (28). Whether there is increased activity of potentially immunogenic proteins in long-term expanded iPSC-derived cell lines is not defined at present. Thus, a periodic analysis of such changes needs to be performed to assure consistency of the genetic profile across specific lots of transplantable cells.

We have previously demonstrated that culturing human ESCs in the presence of animal components, such as mouse feeder cells or bovine albumin, leads to the incorporation of animal molecules in the membranes of human cells (29). These molecules, such as *N*-glycolylneuraminic acid (Neu5Gc), contaminated human ESCs and initiated an antibody-mediated complement deposition when the cells were exposed to human sera. Accordingly, in our current study, to avoid the contamination of generated iPSCs by nonporcine animal component(s), we have used porcine fetal skin-derived fibroblasts as a feeder layer, and no serum derived from other animal species was used. Thus, the derived iPSC-NPCs had no nonporcine elements in their membranes that can elicit an immune reaction in the syngeneic or allogeneic graft recipients.

Previous studies reported the transplantation of iPSC-derived dopaminergic precursors using intrastriatal autologous or allogeneic grafting in nonhuman primates without immunosuppression (30, 31). Minimal or no immune response was seen in autologous grafts, whereas a progressive acquired immune response was seen in allogeneic graft recipients at 3.5 to 4 months after cell grafting. We show that the transient immunosuppression protocol used in our current study is effective in inducing a long-term graft tolerance in allogeneic spinally injured and SLA-mismatched recipients. These results are similar to our previously reported data that demonstrate tolerance across a two-haplotype, fully MHC-mismatched barrier in miniature swine renal allografts after transient (12 days) high-dose treatment with tacrolimus (32). More recently, a functional engraftment of allogeneic iPSC-derived cardiomyocytes after a direct

intramyocardial injection in the cynomolgus monkey model of myocardial infarction was reported. In this experiment, continuous immunosuppression with tacrolimus was used (33). Other groups have reported on the functional benefit after spinal grafting of human iPSC-NPCs in mouse and marmoset spinal injury models (34, 35) and also demonstrated low immunogenicity of mouse iPSC-NPCs (36, 37).

Because the spinal cord and brain represent sites of immune privilege, it has long been speculated that only transient immune suppression is sufficient to ensure long-term engraftment of human fetal tissue-derived or iPSC-NPCs in human allogeneic graft recipients. Thus, our findings demonstrate in a large-animal model of spinal cord traumatic injury that, in fact, a transient 4-week immunosuppression is effective in inducing immune tolerance against allogeneic iPSC-NPC grafts. One limitation of our current study is that a relatively short postgrafting period of survival was used in the pig component of the study. Accordingly, a prolonged postgrafting survival likely exceeding 1 year will be needed to confirm a permanent iPSC-NPC engraftment once cells are grafted into syngeneic or allogeneic transiently immunosuppressed recipients.

Our preclinical large-animal model system will allow us to establish prospective assays to predict graft rejection in the context of autologous, syngeneic, or allogeneic grafting of iPSC-derived neural precursors in naïve or previously injured spinal cord. Similar to the studies from Zhao *et al.* (25), we expect that a profiling of gene regulation, membrane-bound, and soluble-releasable proteins that have immunogenic properties, and recipient T cell activation assays, will be important in determining the immunogenicity of prospective iPSC-derived lineage-committed cell lines to be used for *in vivo* grafting. In this manner, the degree of immune suppression could be personalized to the quantity of recipient T cell reactivity to graft antigens, thereby ensuring that appropriate immune suppression is used.

MATERIAL AND METHODS

Study design

This study was designed to characterize the survival of porcine iPSC-NPCs after spinal grafting in adult naïve syngeneic (nonimmunosuppressed) or chronic spinally injured allogeneic (transiently immunosuppressed) pigs. To generate pluripotent cells, we used Sendai virus encoding four reprogramming factors to reprogram adult pig fibroblasts (harvested from inbred SLA-matched pigs) *in vitro*. The pluripotent nature of established iPSC colonies was determined by *in vitro* induction into all three germ layers (ectoderm, mesoderm, and endoderm) and by the formation of *in vivo* teratoma. NPCs were then induced from pluripotent colonies using the NSC induction protocol and established NPCs characterized *in vitro* and *in vivo* by the following: (i) expression of NPCs markers (flow cytometry or indirect immunofluorescence), (ii) ability of neurons to spontaneously depolarize after long-term *in vitro* induction (Ca²⁺ oscillation), and (iii) ability of iPSC-derived neurons to generate action potential in *ex vivo* striatal slices. To study a multipotent potential of established iPSC-NPCs (SYN-EGFP) grafted into rat striata, we used immunofluorescence staining using neuronal and glial markers and mRNA sequencing using bioinformatics protocol that separates the pig mRNA sequence reads from the host rat mRNA reads. Neurotransmitter phenotype of grafted iPSC-NPC-derived neurons was studied in EGFP⁺ grafts in rat striata and pig spinal cord by immunofluores-

cence staining with pre- and postsynaptic markers specific for inhibitory or excitatory neuronal phenotype.

For quantitative analysis of immune response markers (CD45 and CD8), spinal cord sections taken from iPSC-NPC-grafted (i) syngeneic pigs, (ii) allogeneic pigs at the end of 4 weeks immunosuppression, and (iii) allogeneic pigs at 2.5 months after immunosuppression was terminated, were used. The presence of positively stained CD45 and CD8 cells was analyzed separately in the EGFP⁺ grafts and in surrounding host tissue.

Full details on the methods of *in vitro* iPSC and iPSC-NPC generation/characterization and *in vivo* iPSC-NPC grafting and postmortem analysis can be found in the Supplementary Materials.

Statistical analysis

For statistical analysis, the number of positively stained (CD45⁺ and CD8⁺) cells in allogeneic animals (pigs) with continuous and transient immunosuppression was compared using unpaired, two-tailed Student's *t* test for single comparisons. Data were considered significantly different if *P* < 0.05. GraphPad Prism software was used to run Student's *t* test.

SUPPLEMENTARY MATERIALS

www.sciencetranslationalmedicine.org/cgi/content/full/10/440/eaam6651/DC1

Materials and Methods

Fig. S1. Porcine fibroblast-derived iPSCs generate ectoderm, mesoderm, and endoderm cell derivatives *in vitro* and *in vivo*.

Fig. S2. Previously frozen, *in vitro*-expanded porcine iPSC-NPCs show stable karyotype and generate neural derivatives (neurons, astrocytes, and oligodendrocytes) after *in vitro* induction.

Fig. S3. Long-term grafted (7 to 10 months) porcine iPSC-NPCs in rat striata show protein- and mRNA-defined signature that is consistent with mature porcine CNS tissue.

Fig. S4. Porcine iPSC-NPCs grafted into rat striata show no tumor formation and incomplete myelination at 7 months after grafting.

Fig. S5. Porcine iPSC-NPC-EGFP⁺ grafts in rat striata show normal vascularization and no changes in tumor suppressors or proto-oncogenes at 7 to 10 months after grafting.

Fig. S6. iPSC-NPCs grafted into syngeneic pig spinal cord in the absence of immunosuppression show long-term survival and neuronal and glial differentiation at 3 months after transplantation.

Fig. S7. Porcine iPSC-NPCs grafted spinally in allogeneic, transiently immunosuppressed (1-month immunosuppression) pigs with previous spinal traumatic injury show neuronal and glial differentiation at 3.5 months after grafting.

Fig. S8. Spinally grafted iPSC-NPCs in allogeneic, spinally injured pig with transient immunosuppression (1 month) show extensive neuronal (NeuN) differentiation at 3.5 months after grafting.

Fig. S9. iPSC-NPCs grafted spinally in allogeneic pig with previous spinal injury do not form tumors and show incomplete myelination at 3.5 months after grafting.

Fig. S10. Reprogramming factors (*OCT4* and *KLF4*) are silenced in mature iPSC-NPC grafts in rat striata or spinal cord in allogeneic pig with previous spinal traumatic injury.

Fig. S11. Long-term grafted iPSC-NPCs in rat striata or spinal cord of allogeneic pig show only occasional presence of Sendai virus-associated protein in grafted cells and show no change in expression of immunogenic genes.

Table S1. Quantitative analysis of neuronal and glial differentiation in EGFP grafts.

Table S2. Electrophysiological properties of three transplanted iPSC neurons into the striatum of a rat at 8 months after grafting.

Table S3. mRNA-sequencing species sorting quantification.

Table S4. SLA genotypes of the iPSC-NPC donor and the allogeneic graft recipients.

Table S5. Antibodies used for flow cytometry and immunofluorescence staining.

Appendix S1. Porcine gene list.

REFERENCES AND NOTES

1. K. Takahashi, S. Yamanaka, Induction of pluripotent stem cells from mouse embryonic and adult fibroblast cultures by defined factors. *Cell* **126**, 663–676 (2006).
2. K. Takahashi, K. Tanabe, M. Ohnuki, M. Narita, T. Ichisaka, K. Tomoda, S. Yamanaka, Induction of pluripotent stem cells from adult human fibroblasts by defined factors. *Cell* **131**, 861–872 (2007).

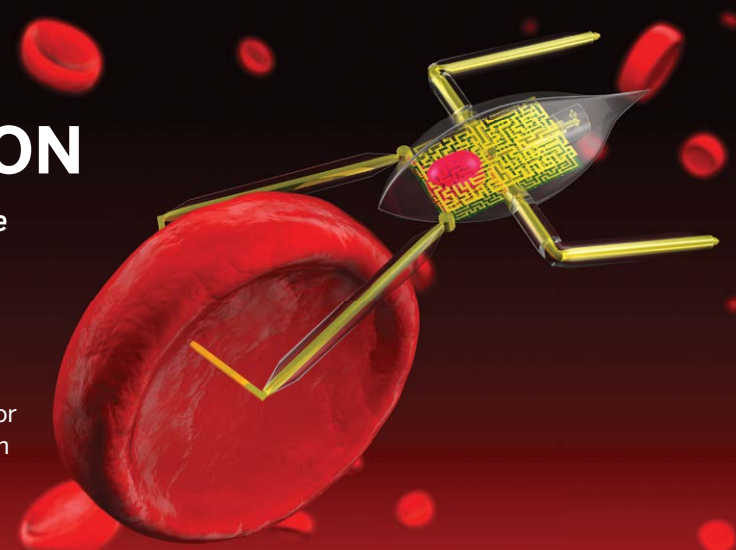
3. M. C. Marchetto, K. J. Brennand, L. F. Boyer, F. H. Gage, Induced pluripotent stem cells (iPSCs) and neurological disease modeling: Progress and promises. *Hum. Mol. Genet.* **20**, R109–R115 (2011).
4. A. R. Muotri, Modeling epilepsy with pluripotent human cells. *Epilepsy Behav.* **14**, (Suppl. 1) 81–85 (2009).
5. R. M. Roberts, B. P. V. L. Telugu, T. Ezashi, Induced pluripotent stem cells from swine (*Sus scrofa*): Why they may prove to be important. *Cell Cycle* **8**, 3078–3081 (2009).
6. B. P. V. L. Telugu, T. Ezashi, R. M. Roberts, Porcine induced pluripotent stem cells analogous to naive and primed embryonic stem cells of the mouse. *Int. J. Dev. Biol.* **54**, 1703–1711 (2010).
7. B. P. V. L. Telugu, T. Ezashi, R. M. Roberts, The promise of stem cell research in pigs and other ungulate species. *Stem Cell Rev.* **6**, 31–41 (2010).
8. M. A. Esteban, J. Xu, J. Yang, M. Peng, D. Qin, W. Li, Z. Jiang, J. Chen, K. Deng, M. Zhong, J. Cai, L. Lai, D. Pei, Generation of induced pluripotent stem cell lines from Tibetan miniature pig. *J. Biol. Chem.* **284**, 17634–17640 (2009).
9. M. A. Esteban, M. Peng, Z. Deli, J. Cai, J. Yang, J. Xu, L. Lai, D. Pei, Porcine induced pluripotent stem cells may bridge the gap between mouse and human iPSC. *IUBMB Life* **62**, 277–282 (2010).
10. T. Ezashi, B. P. V. L. Telugu, A. P. Alexenko, S. Sachdev, S. Sinha, R. M. Roberts, Derivation of induced pluripotent stem cells from pig somatic cells. *Proc. Natl. Acad. Sci. U.S.A.* **106**, 10993–10998 (2009).
11. Z. Wu, J. Chen, J. Ren, L. Bao, J. Liao, C. Cui, L. Rao, H. Li, Y. Gu, H. Dai, H. Zhu, X. Teng, L. Cheng, L. Xiao, Generation of pig induced pluripotent stem cells with a drug-inducible system. *J. Mol. Cell Biol.* **1**, 46–54 (2009).
12. N. Fusaki, H. Ban, A. Nishiyama, K. Saeki, M. Hasegawa, Efficient induction of transgene-free human pluripotent stem cells using a vector based on Sendai virus, an RNA virus that does not integrate into the host genome. *Proc. Jpn. Acad. Ser. B Phys. Biol. Sci.* **85**, 348–362 (2009).
13. D. Usvald, P. Vodicka, J. Hlucilova, R. Prochazka, J. Motlik, J. Strnadel, K. Kucharova, K. Johe, S. Marsala, M. Scadeng, O. Kakinohana, R. Navarro, M. Santa, M. P. Hefferan, T. L. Yaksh, M. Marsala, Analysis of dosing regimen and reproducibility of intraspinal grafting of human spinal stem cells in immunosuppressed minipigs. *Cell Transplant.* **19**, 1103–1122 (2010).
14. C. S. Ho, J. K. Lunney, M. H. Franzo-Romain, G. W. Martens, Y.-J. Lee, J.-H. Lee, M. Wysocki, R. R. Rowland, D. M. Smith, Molecular characterization of swine leukocyte antigen class I genes in outbred pig populations. *Anim. Genet.* **40**, 468–478 (2009).
15. C. S. Ho, J. K. Lunney, J.-H. Lee, M. H. Franzo-Romain, G. W. Martens, R. R. Rowland, D. M. Smith, Molecular characterization of swine leukocyte antigen class II genes in outbred pig populations. *Anim. Genet.* **41**, 428–432 (2010).
16. F. Barnabé-Heider, C. Göritz, H. Sabelström, H. Takebayashi, F. W. Pfrieger, K. Meletis, J. Frisén, Origin of new glial cells in intact and injured adult spinal cord. *Cell Stem Cell* **7**, 470–482 (2010).
17. C. S. Ho, M. H. Franzo-Romain, Y. J. Lee, J. H. Lee, D. M. Smith, Sequence-based characterization of swine leukocyte antigen alleles in commercially available porcine cell lines. *Int. J. Immunogenet.* **36**, 231–234 (2009).
18. C.-S. Ho, E. S. Rochelle, G. W. Martens, L. B. Schook, D. M. Smith, Characterization of swine leukocyte antigen polymorphism by sequence-based and PCR-SSP methods in Meishan pigs. *Immunogenetics* **58**, 873–882 (2006).
19. D. M. Smith, G. W. Martens, C. S. Ho, J. M. Asbury, DNA sequence based typing of swine leukocyte antigens in Yucatan miniature pigs. *Xenotransplantation* **12**, 481–488 (2005).
20. C. S. Ho, G. W. Martens, M. S. Amoss Jr., L. Gomez-Raya, C. W. Beattie, D. M. Smith, Swine leukocyte antigen (SLA) diversity in Sinclair and Hanford swine. *Dev. Comp. Immunol.* **34**, 250–257 (2010).
21. S. E. Essler, W. Ertl, J. Deutsch, B. C. Ruetgen, S. Groiss, M. Stadler, B. Wyszoudil, W. Gerner, C.-S. Ho, A. Saalmueller, Molecular characterization of swine leukocyte antigen gene diversity in purebred Pietrain pigs. *Anim. Genet.* **44**, 202–205 (2013).
22. Y. J. Lee, K. H. Cho, M. J. Kim, D. M. Smith, C. S. Ho, K. C. Jung, D. I. Jin, C. S. Park, J. T. Jeon, J. H. Lee, Sequence-based characterization of the eight SLA loci in Korean native pigs. *Int. J. Immunogenet.* **35**, 333–334 (2008).
23. H.-O. Cho, C.-S. Ho, Y.-J. Lee, I.-C. Cho, S.-S. Lee, M.-S. Ko, C. Park, D. M. Smith, J.-T. Jeon, J.-H. Lee, Establishment of a resource population of SLA haplotype-defined Korean native pigs. *Mol. Cells* **29**, 493–499 (2010).
24. R. Navarro, S. Juhas, S. Keshavarzi, J. Juhasova, J. Motlik, K. Johe, S. Marsala, M. Scadeng, P. Lazar, Z. Tomori, G. Schulteis, M. Beattie, J. D. Ciacchi, M. Marsala, Chronic spinal compression model in minipigs: A systematic behavioral, qualitative, and quantitative neuropathological study. *J. Neurotrauma* **29**, 499–513 (2012).
25. T. Zhao, Z.-N. Zhang, Z. Rong, Y. Xu, Immunogenicity of induced pluripotent stem cells. *Nature* **474**, 212–215 (2011).
26. M. C. N. Marchetto, G. W. Yeo, O. Kainohana, M. Marsala, F. H. Gage, A. R. Muotri, Transcriptional signature and memory retention of human-induced pluripotent stem cells. *PLOS ONE* **4**, e7076 (2009).
27. M. H. Chin, M. J. Mason, W. Xie, S. Volinia, M. Singer, C. Peterson, G. Ambartsumyan, O. Aimiwu, L. Richter, J. Zhang, I. Khvorostov, V. Ott, M. Grunstein, N. Lavon, N. Benvenisty, C. M. Croce, A. T. Clark, T. Baxter, A. D. Pyle, M. A. Teitell, M. Pelegri, K. Plath, W. E. Lowry, Induced pluripotent stem cells and embryonic stem cells are distinguished by gene expression signatures. *Cell Stem Cell* **5**, 111–123 (2009).
28. A. Gore, Z. Li, H.-L. Fung, J. E. Young, S. Agarwal, J. Antosiewicz-Bourget, I. Canto, A. Giorgetti, M. A. Israel, E. Kiskinis, J.-H. Lee, Y.-H. Loh, P. D. Manos, N. Montserrat, A. D. Panopoulos, S. Ruiz, M. L. Wilbert, J. Yu, E. F. Kirkness, J. C. I. Belmonte, D. J. Rossi, J. A. Thomson, K. Eggan, G. Q. Daley, L. S. B. Goldstein, K. Zhang, Somatic coding mutations in human induced pluripotent stem cells. *Nature* **471**, 63–67 (2011).
29. M. J. Martin, A. Muotri, F. Gage, A. Varki, Human embryonic stem cells express an immunogenic nonhuman sialic acid. *Nat. Med.* **11**, 228–232 (2005).
30. A. Morizane, D. Doi, T. Kikuchi, K. Okita, A. Hotta, T. Kawasaki, T. Hayashi, H. Onoe, T. Shiina, S. Yamanaka, J. Takahashi, Direct comparison of autologous and allogeneic transplantation of iPSC-derived neural cells in the brain of a non-human primate. *Stem Cell Reports* **1**, 283–292 (2013).
31. A. Morizane, T. Kikuchi, T. Hayashi, H. Mizuma, S. Takara, H. Doi, A. Mawatari, M. F. Glasser, T. Shiina, H. Ishigaki, Y. Itoh, K. Okita, E. Yamasaki, D. Doi, H. Onoe, K. Ogasawara, S. Yamanaka, J. Takahashi, MHC matching improves engraftment of iPSC-derived neurons in non-human primates. *Nat. Commun.* **8**, 385 (2017).
32. R. Utsugi, R. N. Barth, H. Kitamura, J. Ambroz, D. H. Sachs, K. Yamada, Tolerance across a two-haplotype, fully MHC-mismatched barrier induced in miniature swine renal allografts treated with a 12-day course of tacrolimus. *Transplant. Proc.* **33**, 101 (2001).
33. Y. Shiba, T. Gomibuchi, T. Seto, Y. Wada, H. Ichimura, Y. Tanaka, T. Ogasawara, K. Okada, N. Shiba, K. Sakamoto, D. Ido, T. Shiina, M. Ohkura, J. Nakai, N. Uno, Y. Kazuki, M. Oshimura, I. Minami, U. Ikeda, Allogeneic transplantation of iPSC cell-derived cardiomyocytes regenerates primate hearts. *Nature* **538**, 388–391 (2016).
34. S. Nori, Y. Okada, A. Yasuda, O. Tsuji, Y. Takahashi, Y. Kobayashi, K. Fujiyoshi, M. Koike, Y. Uchiyama, E. Ikeda, Y. Toyama, S. Yamanaka, M. Nakamura, H. Okano, Grafted human-induced pluripotent stem-cell-derived neurospheres promote motor functional recovery after spinal cord injury in mice. *Proc. Natl. Acad. Sci. U.S.A.* **108**, 16825–16830 (2011).
35. Y. Kobayashi, Y. Okada, G. Itakura, H. Iwai, S. Nishimura, A. Yasuda, S. Nori, K. Hikishima, T. Konomi, K. Fujiyoshi, O. Tsuji, Y. Toyama, S. Yamanaka, M. Nakamura, H. Okano, Pre-evaluated safe human iPSC-derived neural stem cells promote functional recovery after spinal cord injury in common marmoset without tumorigenicity. *PLOS ONE* **7**, e52787 (2012).
36. G. Itakura, M. Ozaki, N. Nagoshi, S. Kawabata, Y. Nishiyama, K. Sugai, T. Iida, R. Kashiwagi, T. Ookubo, K. Yastake, K. Matsubayashi, J. Kohyama, A. Iwanami, M. Matsumoto, M. Nakamura, H. Okano, Low immunogenicity of mouse induced pluripotent stem cell-derived neural stem/progenitor cells. *Sci. Rep.* **7**, 12996 (2017).
37. H. Okano, M. Nakamura, K. Yoshida, Y. Okada, O. Tsuji, S. Nori, E. Ikeda, S. Yamanaka, K. Miura, Steps toward safe cell therapy using induced pluripotent stem cells. *Circ. Res.* **112**, 523–533 (2013).

Acknowledgments: We thank the following people for their technical assistance during rat and minipig surgeries and postoperative animal care: C. Santucci, S. Nguyen, A. Smith, K. Osborn, K. Jenne, J. Fujimoto, S. Leonhard, M. Hardee, J. Maryo, M. Yamamoto, C. Bennett, L. Teare, M. Bokar, J. Ring, A. Guardado, D. Dunne, and A. Millen for her help with manuscript preparation. We also thank N. Varki for her neuropathological expertise and help in evaluating H&E-stained slides. **Funding:** J.S. and M.H.-P. were partially supported by the California Institute for Regenerative Medicine (CIRM) Comprehensive Grant and Immunology-Transplantation grant (RC1-00131-1; RM1-01720; M.M. and J.B.) and Sanford Consortium for Regenerative Medicine (SANPORC; M.M.). J.S. was partially supported by the Czech Academy of Sciences (Institutional Research Plan, Institute of Animal Physiology and Genetics no. AV050450515). University of California, San Diego (UCSD) Neuroscience Microscopy Facility was supported by the NIH (NS047101). S.J., J.J., and J.K. were partially supported by the National Sustainability Program I, project number LO1609 (Czech Ministry of Education, Youth and Sports), and RVO: 67985904. A.M. was partially supported by NIH (PO1-HL066941). J.B. is also supported by NIH grants (CA157885 and CA128893). A.R.M. is supported by grants from the CIRM TR2-01814 and TR4-06747, the NIH through R21MH107771, R01MH094753, and U19MH107367, and a NARSAD (National Alliance for Research on Schizophrenia and Depression) Independent Investigator grant to A.R.M. M.M. was supported by NIH (R01OD018272). **Author contributions:** J.S., C.C., S.M., T.K.J., D.B., M.H.-P., and J.K. performed the in vitro experiments. C.B. and O.P. performed the in vitro electrophysiology experiments. A.M. developed and characterized HIV1 vectors. S.P.D., T.D.G., and S.L.P. performed and analyzed the mRNA-sequencing experiment. M.N. and P.C. performed immunofluorescence staining and microscopy imaging. A.N.G., J.K., T.T., K.K., T.Y., S.J., J.J., J.C., M.P.H. and E.C. performed in vivo cell grafting. C.-S.H. and T.K. performed SLA genotyping and contributed to the writing of the paper. A.J.T., F.H.G., J.B., K.Y., and A.R.M. contributed to the design and writing of the paper. M.M. designed the experiment, provided funding, and wrote the paper. **Competing interests:** M.M. is the scientific founder of Neurgain

Technologies Inc. and has an equity interest in the company. In addition, M.M. serves as a consultant to Neurgain Technologies Inc. and receives compensation for these services. The terms of this arrangement have been reviewed and approved by the UCSD in accordance with its conflict of interest policies. A.R.M. is a cofounder and has equity interest in TISMOO, a company dedicated to genetic analysis focusing on therapeutic applications customized for autism spectrum disorder and other neurological disorders with genetic origins. The terms of this arrangement have been reviewed and approved by the UCSD in accordance with its conflict of interest policies. All other authors declare that they have no competing interest(s). **Data and materials availability:** Requests for the porcine iPSCs and the porcine mRNA-sequencing data should be directed to M.M. (mmarsala@ucsd.edu) and S.L.P. (pfaff@salk.edu) and will be supplied upon completion of a material transfer agreement, which will contain a description of the proposed research using the materials and the data.

Submitted 25 December 2016
 Resubmitted 17 November 2017
 Accepted 19 April 2018
 Published 9 May 2018
 10.1126/scitranslmed.aam6651

Citation: J. Strnadel, C. Carromeu, C. Bardy, M. Navarro, O. Platoshyn, A. N. Glud, S. Marsala, J. Kafka, A. Miyanojara, T. Kato Jr., T. Tadokoro, M. P. Hefferan, K. Kamizato, T. Yoshizumi, S. Juhas, J. Juhasova, C.-S. Ho, T. Kheradmand, P. Chen, D. Bohaciakova, M. Hruska-Plochan, A. J. Todd, S. P. Driscoll, T. D. Glenn, S. L. Pfaff, J. Klima, J. Ciacci, E. Curtis, F. H. Gage, J. Bui, K. Yamada, A. R. Muotri, M. Marsala, Survival of syngeneic and allogeneic iPSC-derived neural precursors after spinal grafting in minipigs. *Sci. Transl. Med.* **10**, eam6651 (2018).



**THIS IS NOT
SCIENCE FICTION**

This is captivating, impactful Science

Contact us today to discuss pricing options for adding any of these journals to your collection of Science resources.

Institutional Licensing
 ScienceMag.org/licensing | scienceonline@aaas.org
 1-866-265-4152 (USA) | +1-202-326-6730 (outside USA)

Science
 AAAS

Science
 Advances

Science
 Immunology

Science
 Robotics

Science
 Signaling

Science
 Translational
 Medicine

BONE

Mechanobiologically Optimized 3D Titanium-Mesh Scaffolds Enhance Bone Regeneration in Critical Segmental Defects in Sheep

Anne-Marie Pobloth *et al.*

Citation

Sci. Transl. Med. 10 Jan 2018:
Vol. 10, Issue 423, eaam8828
10.1126/scitranslmed.aam8828

Three-dimensional (3D) titanium-mesh scaffolds offer many advantages over autologous bone grafting for the regeneration of challenging large segmental bone defects. Our study supports the hypothesis that endogenous bone defect regeneration can be promoted by mechanobiologically optimized Ti-mesh scaffolds. Using finite element techniques, two mechanically distinct Ti-mesh scaffolds were designed in a honeycomb-like configuration to minimize stress shielding while ensuring resistance against mechanical failure. Scaffold stiffness was altered through small changes in the strut diameter only. Honeycombs were aligned to form three differently oriented channels (axial, perpendicular, and tilted) to guide the bone regeneration process. The soft scaffold (0.84 GPa stiffness) and a 3.5-fold stiffer scaffold (2.88 GPa) were tested in a critical size bone defect model *in vivo* in sheep. To verify that local scaffold stiffness could enhance healing, defects were stabilized with either a common locking compression plate that allowed dynamic loading of the 4-cm defect or a rigid custom-made plate that mechanically shielded the defect. Lower stress shielding led to earlier defect bridging, increased endochondral bone formation, and advanced bony regeneration of the critical size defect. This study demonstrates that mechanobiological optimization of 3D additive manufactured Ti-mesh scaffolds can enhance bone regeneration in a translational large animal study.

CELL ENGINEERING

Synthetic Biology-Based Cellular Biomedical Tattoo for Detection of Hypercalcemia Associated with Cancer

Aizhan Tastanova *et al.*

Citation

Sci. Transl. Med. 18 Apr 2018:
Vol. 10, Issue 437, eaap8562
10.1126/scitranslmed.aap8562

Diagnosis marks the beginning of any successful therapy. Because many medical conditions progress asymptotically over extended periods of time, their timely diagnosis remains difficult, and this adversely affects patient prognosis. Focusing on hypercalcemia associated with cancer, we aimed to develop a synthetic biology-inspired biomedical tattoo using engineered cells that would (i) monitor long-term blood calcium concentration, (ii) detect onset of mild hypercalcemia, and (iii) respond via subcutaneous accumulation of the black pigment melanin to form a visible tattoo. For this purpose, we designed cells containing an ectopically expressed calcium-sensing receptor rewired to a synthetic signaling cascade that activates expression of transgenic tyrosinase, which produces melanin in response to persistently increased blood Ca^{2+} . We confirmed that the melanin-generated color change produced by this biomedical tattoo could be detected with the naked eye and optically quantified. The system was validated in wild-type mice bearing subcutaneously implanted encapsulated engineered cells. All animals inoculated with hypercalcemic breast and colon adenocarcinoma cells developed tattoos, whereas no tattoos were seen in animals inoculated with normocalcemic tumor cells. All tumor-bearing animals remained asymptomatic throughout the 38-day experimental period. Although hypercalcemia is also associated with other pathologies, our findings demonstrate that it is possible to detect hypercalcemia associated with cancer in murine models using this cell-based diagnostic strategy.

TISSUE ENGINEERING

Computational Modeling Guides Tissue Engineered Heart Valve Design for Long-Term in Vivo Performance in a Translational Sheep Model

Maximilian Y. Emmert *et al.***Citation**

Sci. Transl. Med. 09 May 2018;
Vol. 10, Issue 440, eaan4587
10.1126/scitranslmed.aan4587

Valvular heart disease is a major cause of morbidity and mortality worldwide. Current heart valve prostheses have considerable clinical limitations due to their artificial, nonliving nature without regenerative capacity. To overcome these limitations, heart valve tissue engineering (TE) aiming to develop living, native-like heart valves with self-repair, remodeling, and regeneration capacity has been suggested as next-generation technology. A major roadblock to clinically relevant, safe, and robust TE solutions has been the high complexity and variability inherent to bioengineering approaches that rely on cell-driven tissue remodeling. For heart valve TE, this has limited long-term performance in vivo because of uncontrolled tissue remodeling phenomena, such as valve leaflet shortening, which often translates into valve failure regardless of the bioengineering methodology used to develop the implant. We tested the hypothesis that integration of a computationally inspired heart valve design into our TE methodologies could guide tissue remodeling toward long-term functionality in tissue-engineered heart valves (TEHVs). In a clinically and regulatory relevant sheep model, TEHVs implanted as pulmonary valve replacements using minimally invasive techniques were monitored for 1 year via multimodal in vivo imaging and comprehensive tissue remodeling assessments. TEHVs exhibited good preserved long-term in vivo performance and remodeling comparable to native heart valves, as predicted by and consistent with computational modeling. TEHV failure could be predicted for nonphysiological pressure loading. Beyond previous studies, this work suggests the relevance of an integrated in silico, in vitro, and in vivo bioengineering approach as a basis for the safe and efficient clinical translation of TEHVs.

TISSUE ENGINEERING

Production and Transplantation of Bioengineered Lung into a Large Animal Model

Joan E. Nichols *et al.***Citation**

Sci. Transl. Med. 01 Aug 2018;
Vol. 10, Issue 452, eaao3926
110.1126.scitranslmed.aao3926

The inability to produce perfusable microvasculature networks capable of supporting tissue survival and of withstanding physiological pressures without leakage is a fundamental problem facing the field of tissue engineering. Microvasculature is critically important for production of bioengineered lung (BEL), which requires systemic circulation to support tissue survival and coordination of circulatory and respiratory systems to ensure proper gas exchange. To advance our understanding of vascularization after bioengineered organ transplantation we produced and transplanted BEL without creation of a pulmonary artery anastomosis in a porcine model. While in bioreactor culture, we facilitated systemic vessel development using growth factor-loaded microparticles. A single pneumonectomy, performed one month prior to BEL implantation, provided the source of autologous cells used to bioengineer the organ on an acellular lung scaffold. During 30 days of bioreactor culture we facilitated systemic vessel development using growth factor-loaded microparticles. We evaluated recipient survival, autograft (BEL) vascular and parenchymal tissue development, graft rejection, and microbiome reestablishment in autografted animals 10 hours, 2 weeks, 1 month and 2 months after transplant. BEL became well vascularized as early as 2 weeks post-transplant and formation of alveolar tissue was observed in all animals ($n = 4$). There was no indication of transplant rejection. BEL continued to develop post-transplant and did not require addition of exogenous growth factors to drive cell proliferation or lung and vascular tissue development. The sterile BEL was seeded and colonized by the bacterial community of the native lung.

Citation

Sci. Transl. Med. 18 Jan 2017:
Vol. 9, Issue 373, eaaf3925
10.1126/scitranslmed.aaf3925

CARDIOVASCULAR DISEASE: Soft Robotic Sleeve Supports Heart Function

Ellen T. Roche, Markus A. Horvath, Isaac Wamala, Ali Alazmani, Sang-Eun Song, William Whyte, Zurab Machaidze, Christopher J. Payne, James C. Weaver, Gregory Fishbein, Joseph Kuebler, Nikolay V. Vasilyev, David J. Mooney, Frank A. Pigula, and Conor J. Walsh

Citation

Sci. Transl. Med. 01 Mar 2017:
Vol. 9, Issue 379, eaah4586
10.1126/scitranslmed.aah4586

NANOTECHNOLOGY: Improved Tissue Cryopreservation Using Inductive Heating of Magnetic Nanoparticles

Navid Manuchehrabadi, Zhe Gao, Jinjin Zhang, Hattie L. Ring, Qi Shao, Feng Liu, Michael McDermott, Alex Fok, Yoed Rabin, Kelvin G. M. Brockbank, Michael Garwood, Christy L. Haynes, and John C. Bischof

Citation

Sci. Transl. Med. 19 Apr 2017:
Vol. 9, Issue 386, eaa19044
10.1126/scitranslmed.aai9044

WOUND HEALING: Glycosaminoglycan-Based Hydrogels Capture Inflammatory Chemokines and Rescue Defective Wound Healing in Mice

Nadine Lohmann, Lucas Schirmer, Passant Atallah, Elke Wandel, Ruben A. Ferrer, Carsten Werner, Jan C. Simon, Sandra Franz, and Uwe Freudenberg

Citation

Sci. Transl. Med. 04 Oct 2017:
Vol. 9, Issue 410, eaa17466
10.1126/scitranslmed.aai7466

BIOMATERIALS: Engineering a Highly Elastic Human Protein–Based Sealant for Surgical Applications

Nasim Annabi, Yi-Nan Zhang, Alexander Assmann, Ehsan Shirzaei Sani, George Cheng, Antonio D. Lassaletta, Andrea Vegh, Bijan Dehghani, Guillermo U. Ruiz-Esparza, Xichi Wang, Sidhu Gangadharan, Anthony S. Weiss, and Ali Khademhosseini

Citation

Sci. Transl. Med. 28 Feb 2018:
Vol. 10, Issue 430, eaao3612
10.1126/scitranslmed.aao3612

PRECISION HEALTH: Toward Achieving Precision Health

Sanjiv Sam Gambhir, T. Jessie Ge, Ophir Vermesh, and Ryan Spittler

Citation

Sci. Transl. Med. 04 Apr 2018:
Vol. 10, Issue 435, eaao4097
10.1126/scitranslmed.aao4097

RETINAL DISEASE: A Bioengineered Retinal Pigment Epithelial Monolayer for Advanced, Dry Age-Related Macular Degeneration

Amir H. Kashani, Jane S. Lebkowski, Firas M. Rahhal, Robert L. Avery, Hani Salehi-Had, Wei Dang, Chih-Min Lin, Debbie Mitra, Danhong Zhu, Biju B. Thomas, Sherry T. Hikita, Britney O. Pennington, Lincoln V. Johnson, Dennis O. Clegg, David R. Hinton, and Mark S. Humayun

Citation

Sci. Transl. Med. 25 Apr 2018:
Vol. 10, Issue 438, eaar6076
10.1126/scitranslmed.aar6076

DIAGNOSTICS: A Digital Microfluidic System for Serological Immunoassays in Remote Settings

Alphonsus H. C. Ng, Ryan Fobel, Christian Fobel, Julian Lamanna, Darius G. Rackus, Aimee Summers, Christopher Dixon, Michael D. M. Dryden, Charis Lam, Man Ho, Nooman S. Mufti, Victor Lee, Mohd Afiq Mohd Asri, Edward A. Sykes, M. Dean Chamberlain, Rachael Joseph, Maurice Ope, Heather M. Scobie, Alaine Knipes, Paul A. Rota, Nina Marano, Paul M. Chege, Mary Njuguna, Rosemary Nzunza, Ngina Kisangau, John Kiogora, Michael Karuingi, John Wagacha Burton, Peter Borus, Eugene Lam, and Aaron R. Wheeler

Citation

Sci. Transl. Med. 30 May 2018:
Vol. 10, Issue 443, eaap8373
10.1126/scitranslmed.aap8373

NEUROPROSTHETICS: Proprioception From a Neurally Controlled Lower-Extremity Prosthesis

Tyler R. Clites, Matthew J. Carty, Jessica B. Ullauri, Matthew E. Carney, Luke M. Mooney, Jean-François Duval, Shriya S. Srinivasan, and Hugh. M. Herr

Citation

Sci. Transl. Med. 20 June 2018:
Vol. 10, Issue 446, eaaq1802
10.1126/scitranslmed.aaq1802

TISSUE ENGINEERING: Tissue Engineering Toward Temporomandibular Joint Disc Regeneration

Natalia Vapniarsky, Le W. Huwe, Boaz Arzi, Meghan K. Houghton, Mark E. Wong, James W. Wilson, David C. Hatcher, Jerry C. Hu, and Kyriacos A. Athanasiou